Repeated Measurements of Electrical Contact Resistance between Two Stainless Steel Balls

Sang Kuk Kim

Supervised by

Professor Insuk Yu

A Dissertation

Submitted to the Faculty of

Seoul National University

In Partial Fulfillment of

the Requirements for the Degree of

Doctor of Philosophy

August 2013

Department of Physics and Astronomy
Graduate School
Seoul National University

Abstract

Repeated Measurements of Electrical Contact Resistance between Two Stainless Steel Balls

San Kuk Kim

Department of Physics and Astronomy
Graduate School
Seoul National University

The electrical resistance of the contact is dependent on the bulk electrical resistivity of the contacting materials and the contact parameters, such as contact area, and contact shape. However, if the contact load is very low for two contact members to be separated by a thin oxide layer that is form natively, the electrical contact resistance shows a complicated aspect.

There are two electrical states in a weak contact. One is a high resistance contact, another is a low resistance contact. A high resistance in the weak contact is due to an oxide layer between two contact members. In classical electrodynamics, the electron cannot flow through an oxide layer. On the contrary, in Quantum mechanics, there is some probability finding electrons in the other side of an oxide layer. Such phenomenon called tunneling. The tunneling resistance is very high comparing to that of metal. The low resistance contact is due to the bridge connecting two contact members. If the load applying to the contact is enough high to destroy the oxide layer existing between two contact members, the electrical

resistance of the contact is determined by the bulk electrical resistivity and the contact area. However, in the case of a weak contact, two contact members are separated by a thin oxide layer covering each contact member. In that case, the oxide layer in the contact can be destroyed by electrical impact. Such phenomenon called dielectric breakdown.

The electrical resistance of the contacts between two stainless steel balls was measured in order to study electrical conduction of the contact separated by a thin oxide layer. By repeating the measurements up to 5000 times, the contact resistances were found to have a bimodal log-normal distribution. The higher resistance (~1 MΩ) peak was formed from the tunneling conduction through the thin oxide layer of the contacts, whereas the lower resistance (~10 Ω) peak was due to the conducting bridges formed within the oxide layer when dielectric breakdown occurred at $V_{th} \geq 1$ V. It was possible for a low resistance contact to be made by dielectric breakdown regardless of the mechanical parameters of the contact configuration.

Using random resistor network model with circuit breaker, we simulated the low resistance state. The value of the low resistance contact can be estimated through that of the electrically induced filament bundle, and not by the Holm or the Sharvin equation in the electrical contact theory. We identified that the simulation result agree to our experimental data for appropriate simulation parameters, such as resistor values, current. Especially, the fact that the log normal distribution of the resistance is appeared in the simulation result as well as the experimental result supports our proposition that the low resistance contact is formed electrically, not mechanically.

In addition, we performed several experiments for another condition affecting the electrical contact resistance. The slow variation of electrical contact resistance with the time evolution shows that the interface state, such as the position of defects

existing inside the oxide layer, is changed slowly. The variation of occurrence depending on the atmospheric composition shows the electrical contact is sensitive to the existence of oxygen in the atmosphere.

Keywords: electrical contact resistance, dielectric breakdown, random resistor, tunneling effect, conduction filaments, log-normal distribution

Student number: 2007-30778

Contents

Abstract

List of Figures

List of Tables

1 Introduction 1

2 Theory.....5

2.1 Electrical contact resistance 5

2.2 Electrical contact resistance with a thin oxide layer 12

2.3 Voltage-temperature relation in the contact 17

2.4 Resistance change from high resistance to low resistance.....19

2.5 Log normal distribution of filaments' resistance 26

3 Experimental setup and methods 29

3.1 Properties of type 304 stainless steel 29

3.2 Experimental setup 30

3.3 Experimental method.....31

3.3.1 Distribution of electrical contact resistance 31

3.3.2 I-V measurements.....33

3.4 Simulation.....34

4 Results and discussions.....36

4.1 The distribution of electrical contact resistance.....36

4.1.1 Two kinds of electric contact resistance.....36

4.1.2 The origin of a low and high resistancement.....40

4.2 Time evolution of electrical conact resistance.....44

4.2.1 Slow change of electrical contact resistance.....44

4.2.2 A sudden drop of electrical contact resistance.....47

4.3 I-V characteristic.....51

4.3.1 Diverse I – V characteristics.....51

4.3.2 Dielectric breakdown voltage and its severity.....55

4.3.3 The distribution of electrical resistance after melting.....58

4.4 Dependence on current.....60

4.5 Dependence on an oxide layer thickness.....63

4.5.1 XPS data of Type 304 stainless steel plate after heat treatment.....64

4.5.2 Variation with respect to the oxide layer thickness.....65

4.5.3 Post-breakdown resistance and severity 69

4.6 Dependence on atmosphere.....71

4.7 The result of simulation 74

4.7.1 Distribution 74

4.7.2 I-V characteristic 77

5 Conclusion 81

Bibliography 83

국문 초록 91

List of Figures

2.1 The estimation of apparent contact area.....6

2.2 Three kinds of electrical contact. 7

2.3 A real contact. 9

2.4 The surface simulated by a fractal theory in the reference. 11

2.5 The contact separated by thin oxide layer.....12

2.6 Rectangular barrier V_0>E. 13

2.7 Schematic diagram of tunneling by the magnitude of voltage. 15

2.8 The occurrence of conducting filaments in the interface. 29

2.9 Examples of bond percolation. 21

2.10 Forming the filament in two dimensional stacked layer model.....23

2.11 The log normal distribution of filament bundle's resistance. 27

3.1 Experimental Setup. 30

3.2 The set up of Measuring the distribution of electrical contact resistance.. 32

3.3 The I-V measurements of electrical contact resistance.....33

3.4 Schematic diagram of simulation..... 44

4.1 Electrical contact resistance at current 1 μA..... 37

4.2 Histogram of electrical contact resistance at current 1 μA.. 39

4.3 Distribution of electrical contact resistance at 0.1 and 10 μA..... 41

4.4 XPS depth profile of usual Type 304 stainless steel plate... 43

4.5 Time evolution of contact resistance..... 46

4.6 A sudden change of electrical contact resistance... 48

4.7 The variation of electrical contact resistance by condition change 50

4.8 Fifty and Five representatives of I – V meaasurements..... 54

4.9 The distribution of voltage and resistance after breakdown. 56

4.10 The severity of dielectric breakdown and post-breakdown resistance..... 57

4.11 The distribution of initial and final resistance of I-V measurement..... 59

4.12 The variation of the resistance distribution with respect to current..... 61

4.13 The plot of mean voltage to current. 63

4.14 XPS depth profile of stainless steel with respect to thermal treatment.... 66

4.15 The distribuion of resistance by changing the oxide layer thickness..... 67

4.16 The distribution of breakdown voltage at several-thick oxide layers.. 69

4.17 The dielectric breakdown voltage and Post-breakdown resistance.. 72

4.18 The variation of distribution by changing atmosphere... 73

4.19 The variation of the distribution according to humidity in air.....74

4.20 4 snapshots of simulation... 76

4.21 the distribution of the resistance in simulation.....77

4.22 I-V measurements by simulation.....79

4.23 the snapshots of blue symbol in the figure 4.18... 80

List of Tables

3.1 The estimation of apparent contact area 29

Chapter 1

Introduction

Breakable electrical contacts are ubiquitous (e.g., switches, connectors, plugs, carbon brush, and relays). For example, many people slide their USB memory sticks into a computer every day. Although the connector pins are coated with gold film for preventing the surface from oxidization, one occasionally experiences contact problems [1-5]. Even if an electrical contact is very familiar and well-known subject, it need more research at several studies. For example, the granular system being composed of conducting grains shows a slow relaxation of its whole electrical resistance [6-9]. That is a reflection of packing the granular system with time evolution. Thus, the study of how the resistance of a single contact distributes can become to be a good guidepost for the comprehensive understanding about a conducting granular system.

Contacts are microscopic in nature. Studies have been performed on metal contacts since the 1960s. Formula named after Holm and Sharvin are results of such researches. And they form the basis of many theoretical modeling which provides a good estimation of electrical contact resistance until now [10-19]. And in recent research, a further understanding of electrical contacts through progress in nano-science and technology is reached [20-29]. However, understanding the basic physics behind the contact phenomena is far from complete. Furthermore, the study

on the transition from a high resistance contact state to a low resistance one induced by electrical impact, as opposed to that by mechanical load, is rare. Generally, thin (a few nanometers) dielectric films, e.g., oxides, are present between the contacting surfaces. When a contact is made, the two contacting surfaces are pressed against each other [30-34], and in most cases, the dielectric films are destroyed by high contact pressure. Such cases are well explained by Holm and Sharvin model in conjunction with the fractal surface simulation [35]. On the contrary, if one metal is not faced by the other metal directly, the narrowest gap, which is the smallest distance between contact members, induces quantum mechanical tunneling conduction and the thin dielectric layer may change the conduction [36, 37]. But because the gap between the electrodes is very small, an extremely large electric field can be produced in the dielectric layer even with a minute voltage difference between the electrodes. This electric field can break down the dielectric layer and form conducting bridges completely or partially [38-40] and their shape looks like filament bundle [41-43]. In that case, the electrical resistance of the contact is hard to be explained by the Holm or Sharvin model because of the difficulty of determining the electrical contact area. Thus, a new model about the electrical conduction properties of such contacts is needed other than the models based on the Holm and Sharvin resistance formula. In this study the random circuit breaker model which was applied to the resistive random – access memory (RRAM) materials tried [44-50].

Because identical contacts cannot be generated microscopically, repeating measurements to confirm experimental results is difficult for electrical contacts. Hence, the statistical analysis of the contact ensembles becomes important. For the repeated measurements of electrical contacts, a contact system with sufficient durability and convenience for the repetitive measurements is required. Such

problems are related to the selection of material. Stainless steel balls were chosen because of their mechanical strength, chemical stability and very thin (~ 2.5 to 5 nm) surface oxide layers [51-53].

We studied the electrical conduction properties of the contacts made by vertically stacking two small stainless steel balls. The electrical resistance was measured repeatedly for two stainless steel ball contacts after short periods (0.08 s) of vibrations to break-and-remake the electrical contact. The accelerations of the array were minimized to prevent alterations of the contacting surfaces. Up to 5000 measurements were made to find out the distributions of the contact resistance values. This statistical study gives us interesting information about the distribution of electrical contact resistances, indicating the presence of conduction through bridges as well as the quantum mechanical tunneling through oxide films. If a large bias voltage is applied, the oxide layer can be destroyed by electrical discharge. Otherwise, the oxide layer is still blocking the two contact surfaces. We identify this transition-like phenomenon in the simulation as well as in our experimental results. Furthermore, even after dielectric breakdown occurs, the resistance distribution persist its log-normal shape consistently in simulation and experiment.

Furthermore, we obtained several interesting results about electrical contact. The electrical resistance of the contact is slowly changed with time evolution in common with a granular system. In the case of a high resistance contact, when 1000 seconds passes, its resistance is down about 20%, comparing to its initial resistance. On the contrary, the variation of a low resistance contact to its initial resistance is 1~2%. This result infers that electrical conduction mechanism of two contact states is different. And we found that the electrical contact is sensitive to atmospheric condition around it. Especially, the occurrence of a low resistance contact depends

on the existence of oxygen.

Chapter 2

Theory

2.1 Electrical contact resistance

When two bodies are met close each other, contacts are naturally formed. Usually, the contact surface of each body is deformed by the contact load. And the deformed region is where electrical current flows if we apply potential difference between contact members. Ideally, if the contact area is a point, the electrical contact resistance is infinite [54, 55]. However, the real contact occurs with some area, not a point contact. The relation between the contact load and the contact area has been well established, assuming that the contact is elastic one [30]. Provided that same two circular bodies are contacted elastically and there is no adhesive force between contact surfaces, the relation between the contact load and the contact area is given by the following Hertz formula.

$$a = \left(\frac{3PR}{4E^*}\right)^{1/3}, \frac{1}{E^*} = \frac{2(1-\upsilon^2)}{E} \tag{2.1}$$

In the above equation, a is the circular radius of the contact area, P the contact load, R the radius of each body, E the young's modulus, and υ is the Poisson ratio. This Hertz model of elastic contact provides the size of an apparent contact area, even when the real contact area or electrical contact area is not known well.

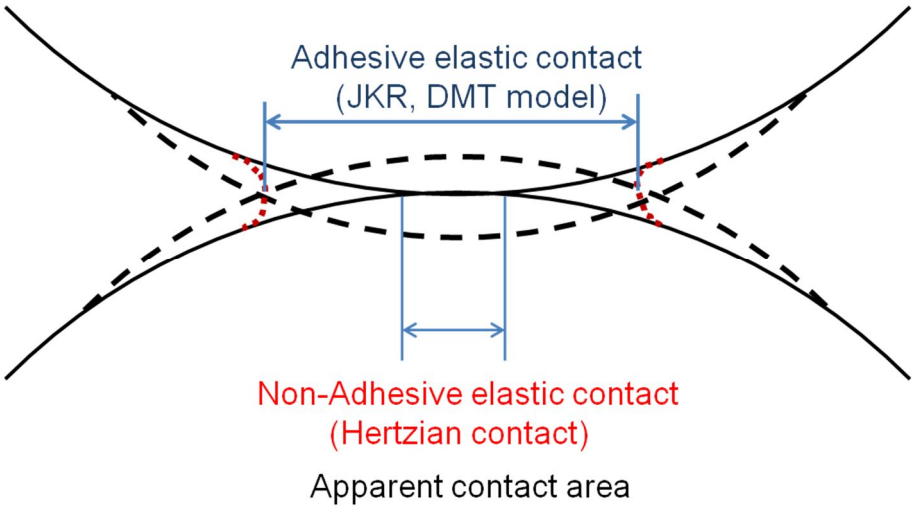

Figure 2.1 | The estimation of apparent contact area. There are two theories in elastic contact: one is adhesive case, another is non-adhesive case.

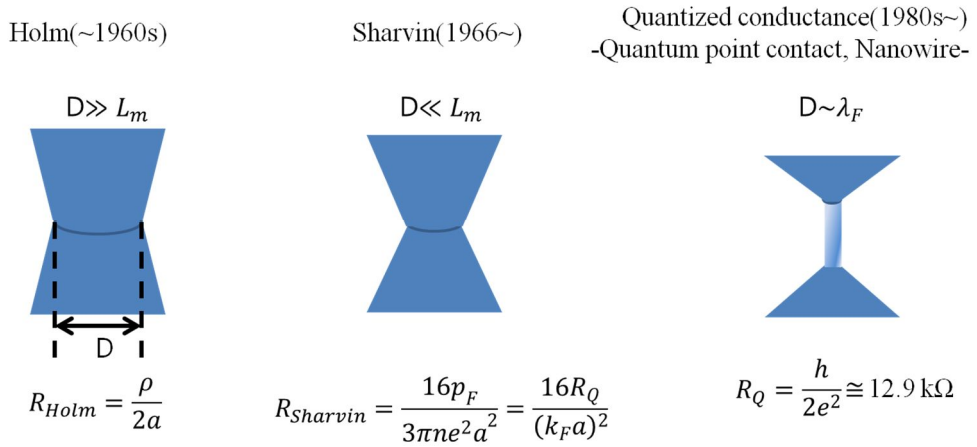

Figure 2.2 | Three kinds of electrical contact. The electrical contact can be divided into three cases according to its size of contact area.

Once the apparent contact area is evaluated, there are three kinds of electrical contact theory according to the size of the contact area.

In the case of a large contact area, whose size is bigger than electron mean free path of contact member, the electrical resistance of contact is inversely proportional to the area of contact. Assuming that two balls are contacted elastically and it forms circular contact area, then the electrical resistance which is called the Holm resistance is

$$R_H = \frac{\rho}{2a}, \tag{2.2}$$

where ρ is the bulk resistivity of contact member and a is the radius of circular contact area [12, 15].

When the size of the contact area is smaller than the electron mean free path of contact members, the electrical resistance of the contact is inversely proportional to the area, the square of radius [14, 56, 57].

$$R_S = \frac{16p_F}{3\pi ne^2a^2} = \frac{16R_Q}{(k_F a)^2} \ , \ R_Q = \frac{h}{2e^2} \simeq 12.9 \ \text{k}\Omega \tag{2.3}$$

p_F, k_F are Fermi momentum and Fermi wave vector, respectively. n, e are density and charge of electron, h is the Plank constant, and R_Q is the inverse of quantum conductance. R_S that is called as the Shavin resistance is calculated assuming that the electron in the contact region moves without energy loss by collision with scatterers, i.e. in the ballistic regime.

Quantum resistance R_Q in above equation is the quantized conductance that is appeared when the orifice of the contact is comparable to or smaller than the Fermi wavelength of electron in contact material. However, this does not mean that the electrical conductance of one channel have to be the integer multiple of a conductance quantum. It mentions that the electrical resistance of contact is the sum of the channel, which has a conductance quantum, number [20].

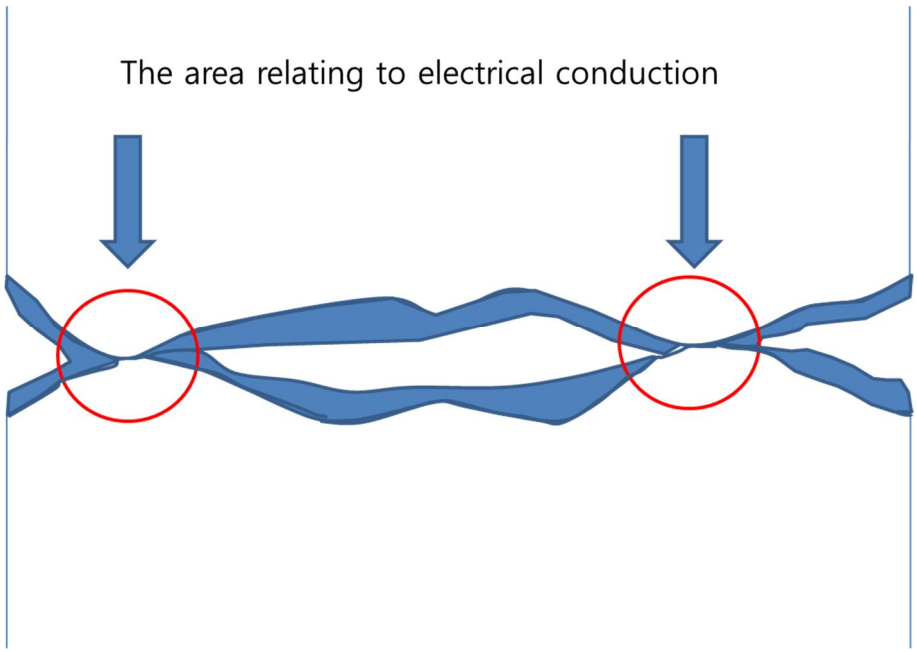

Figure 2.3 | A real contact. Usually, there are many irregularities on the surface of material. Furthermore, the surface is covered with a native oxide layer. That means that the real contact is a complex state, not a simple state.

In real contact, the contact is divided into two regions. One is responsible for electrical conduction and load bearing, another is responsible for only load bearing. Furthermore, this part that is responsible for electrical conduction is not a single point contact, but the union of point contacts with diverse sizes. Such contact has

been realized by statistical method. In that model, the asperity height has some distribution function like Gaussian is assumed, then that surface is met with another flat surface [10, 11, 58-60]. In recent contact mechanics research, a real contact is modeled by using the fractal theory [32, 35, 61-65]. In any case, the contact area facing two surfaces directly includes many spots with diverse sizes.

In electrical contact theory, the electrical contact resistance was calculated with statistical method in which the asperity distribution is assumed by some distribution function. In the 1960s, Williamson assumed that the height distribution of asperity in contacts are exponential and showed that the electrical conductance of such contact is

$$\mathrm{G} \propto \mathrm{A}e^{-h}, \tag{2.4}$$

where A is the nominal contact area (apparent contact area) and h is the fluctuation of the datum line. Yet another result for the contact resistance which was published by Greenwood is

$$\mathrm{R} = \rho\left(\frac{1}{2na} + \frac{1}{2\alpha}\right) \tag{2.5}$$

where ρ is the bulk resistivity of the contact member, n and a are the number and radius of circular electrical spots, and α is the radius of the cluster defined by Holm.

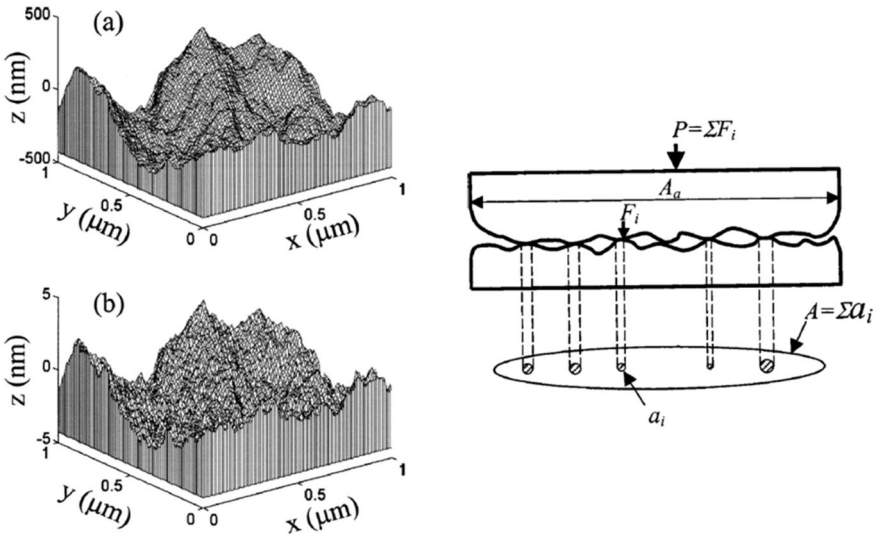

Figure 2.4 | The surface simulated by a fractal theory in the reference [35]. In real contact, the contact includes many spots with diverse sizes.

In recent research, the electrical resistance of the contact is estimated by computer simulation. In that case, the total conductance, which is the inverse of the total resistance, is the sum of the conductance responsible for each spot. The resistance of each spot is calculated by applying the Holm and Sharvin resistance formula to each one according to the spot's size, where the limit area that does not

affect the electrical conduction is assumed [35]. The quantum conductance is not considered in that calculation.

2.2 Electrical contact resistance of a contact separated by thin oxide layer

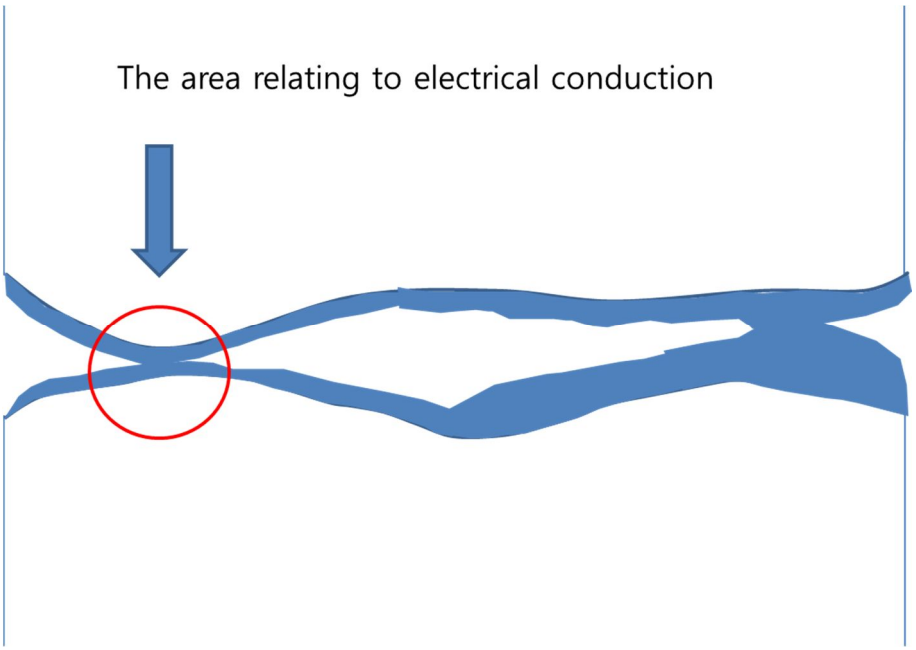

Figure 2.5 | The contact separated by thin oxide layer. Usually, the contact member is covered with a native oxide layer. If the contact load is not enough to destroy the surface oxide layer, the current in the contact perturbed by an oxide layer.

The metal-metal contact is not always made in the real contact. If the oxide layer on the surface of contact member is thick or the contact load is not enough to destroy the oxide layer, the metal surface of one contact member is not directly faced with the metal surface of another contact member. In that case, the electron does not move from one contact member to another classically. But, even if the potential barrier is higher than the energy of the moving electron, the electrical current can flow through a thin layer quantum mechanically.

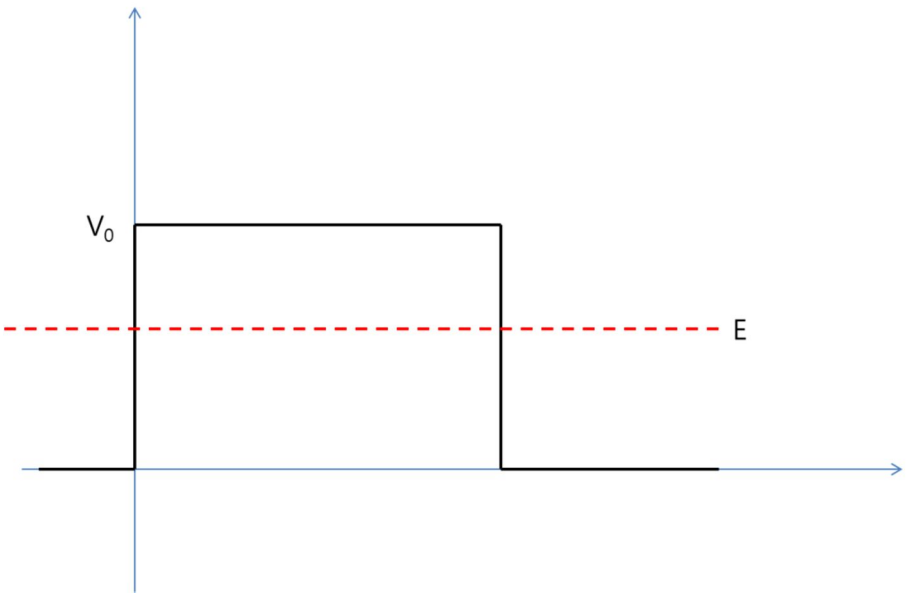

Figure 2.6 | Rectangular barrier V_0>E. V_0 is the barrier height of an insulating layer, E is the energy of the electron. Even if the potential barrier is higher than the energy of the moving electron, the electrical current can flow through a thin layer quantum mechanically.

In usual calculation of tunnel current, a finite square barrier problem is considered for the comprehensive study. Considering a particle with energy $\mathrm{E} = \mathrm{P}^2/(2\mathrm{M})$ is sent to a rectangular barrier with thickness l and height $\mathrm{V}_0(\mathrm{E} < \mathrm{V}_0)$, then the transmission T (tunneling rate) is [66-68]

$$T^{-1} = 1 + \frac{V_0^2}{4E(V_0-E)} sinh^2(\frac{l}{\hbar}\sqrt{2M(V_0-E)}) \tag{2.6}$$

Assuming that the barrier thickness l is varied with Gaussian distribution, the probability distribution $\mathrm{P}_1(\mathrm{T})$ of the transmission T is given by the variable change $\mathrm{P}_1(\mathrm{T}) = \mathrm{P}(\mathrm{l})$.

$$P_1(T) = \frac{\sqrt{B}}{\sqrt{2\pi}}\frac{\lambda}{\sigma}\frac{exp\left[-\frac{\lambda^2}{2\sigma^2}\left(2\,sech^{-1}\left(\sqrt{B\left(\frac{1}{T}-1\right)}\right)-\frac{l_0}{\lambda}\right)^2\right]}{T^2\sqrt{\frac{1}{T}-1}\sqrt{1+B\left(\frac{1}{T}-1\right)}}, \tag{2.7}$$

where

$$\mathrm{B} = \frac{\mathrm{V}_0^2}{4\mathrm{E}(\mathrm{V}_0-\mathrm{E})}, \lambda = \frac{\hbar}{\sqrt{2\mathrm{M}(\mathrm{V}_0-\mathrm{E})}},$$

and l_0, σ are the average value and standard deviation of Gaussian distribution. This probability distribution is can be changed into approximate form in the regime of $T \ll T_B < 1, T_B \equiv \frac{B}{1+B}$

and

$$P_1(t) \simeq \frac{\lambda}{(\sqrt{2\pi}\sigma T)} exp\left[-\frac{\lambda^2}{2\sigma^2}\left(2\,ln\,2\sqrt{B/T} - (l_0/\lambda)\right)^2\right]. \qquad (2.8)$$

It is the probability function of log-normal distribution [69]. That is, the transmission is very low, the current fluctuation with varying thickness of barrier which is a normal distribution, exhibits log-normal distribution.

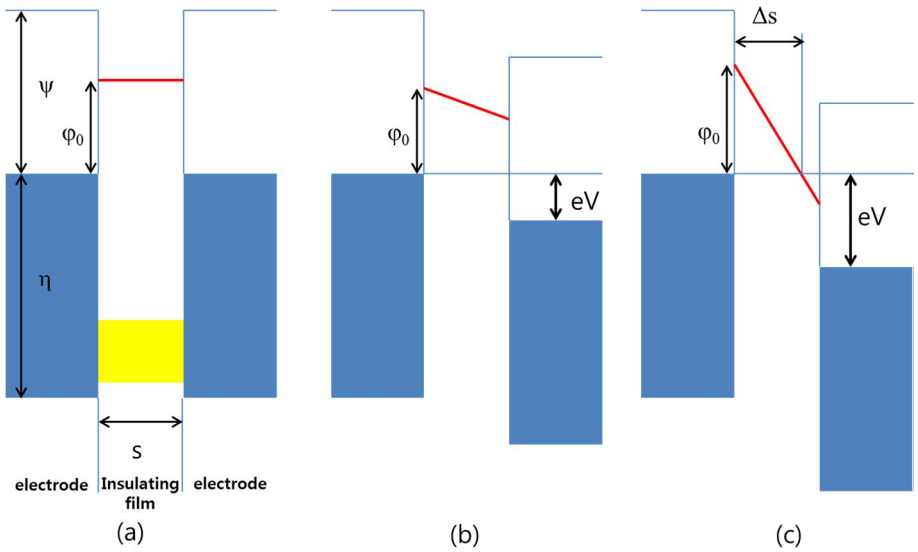

Figure 2.7 | Schematic diagram of tunneling by the magnitude of voltage. Tunneling regimes are divided into three kinds according the external potential difference.

The J-V relation of tunneling current was well researched by Simons [36]. In rectangular barrier, tunnel current is determined by barrier height and thickness of an oxide layer, and the voltage range. He divided voltage level into three regimes.

In low voltage regime: $V \simeq 0$, J is

$$J = \left[\frac{3(2m\varphi_0)^{1/2}}{2s}\right]\left(\frac{e}{h}\right)^2 V exp\left[-\left(\frac{4\pi s}{h}\right)(2m\varphi_0)^{1/2}\right]. \quad (2.10)$$

In this case, the resistance of insulating film is ohmic characteristic, in which it is independent on the voltage, only dependent on the parameter of the insulator.

In intermediate voltage regime: $V < \varphi_0/e$, J is

$$\mathrm{J} = \left(\frac{\mathrm{e}}{2\pi \mathrm{h s}^2}\right)\left\{\left(\varphi_0 - \frac{\mathrm{eV}}{2}\right)\exp\left[-\frac{4\pi \mathrm{s}}{\mathrm{h}}(2\mathrm{m})^{\frac{1}{2}}\left(\varphi_0 - \frac{\mathrm{eV}}{2}\right)^{\frac{1}{2}}\right] - \left(\varphi_0 + \frac{\mathrm{eV}}{2}\right)\exp\left[-\frac{4\pi \mathrm{s}}{\mathrm{h}}(2\mathrm{m})^{\frac{1}{2}}\left(\varphi_0 + \frac{\mathrm{eV}}{2}\right)^{\frac{1}{2}}\right]\right\} \quad (2.11)$$

As shown in this relation, this J-V relation is non-ohmic characteristic. That is, the current is dependent on the voltage applied by external source.

In high voltage regime: $V > \varphi_0/e$, J is

$$\mathrm{J} = \frac{2.2\mathrm{e}^3\mathrm{F}^2}{8\pi \mathrm{h}\varphi_0}\left\{\exp\left[-\frac{4\pi}{2.96\mathrm{heF}}(2\mathrm{m})^{\frac{1}{2}}\varphi_0^{\frac{3}{2}}\right] - (1 + \frac{\mathrm{eV}}{2})\exp\left[-\frac{8\pi}{2.96\mathrm{heF}}(2\mathrm{m})^{\frac{1}{2}}\varphi_0^{\frac{3}{2}}\left(\varphi_0 + \frac{2\mathrm{eV}}{\varphi_0}\right)^{\frac{1}{2}}\right]\right\}$$

(2.12)

where F=V/s is the field strength in the insulator. In the special case of very high voltage: $V > (\eta + \varphi_0)/e$, the second term in the above equation can be ignored. Then, the current density J is changed into

$$J = \frac{2.2e^3F^2}{8\pi h\varphi_0} \exp\left[-\frac{4\pi}{2.96heF}(2m)^{\frac{1}{2}}\varphi_0^{\frac{3}{2}}\right]. \quad (2.13)$$

This equation is similar to field emission current, which is called the Fowler-Nohrheim tunneling equation, except for some factor. In metal – insulator – metal junction, this equation is why the plot of $\ln\frac{J}{V^2}$ vs $\frac{1}{V}$ is drawn to identify tunneling regime.

2.3 Voltage-temperature relation in the contact

It is possible that the temperature of the electrical contact is elevated because of joule heating. And it is competition with thermal transfer toward heat bath, for example the air, the other portion except for electrical contact. If the electrical energy supplied by external source proceeds the thermal transfer toward heat bath, then it is possible that the electrical contact is melted [12, 15, 70].

Assuming that there are two consecutive surfaces which are equipotential

surfaces and the difference of potential is $d\varphi$ and the current, I, flows between two surfaces. The resistance, dR, is $d\varphi/I$. And if there is the temperature difference, dT, between two surfaces, then the equation $-dT = I\varphi dW$ is induced. According to the relation of the power and resistance, $dW = dR/\varrho\lambda$, the temperature variation to the potential difference is $-\varrho\lambda dT = \varphi d\varphi$, where ϱ, λ are the electrical resistivity and thermal conductivity, respectively. Its integration is

$$\int_T^{T_\theta} \varrho\lambda dT` = \frac{1}{2}\varphi^2. \quad (2.14)$$

Using the Weidemann-Franz law, $\varrho\lambda = LT$, in the above equation can be changed into

$$\int_T^{T_\theta} \varrho\lambda dT` = \int_T^{T_\theta} LT dT` = \frac{1}{2}L(T_\theta^2 - T^2) = \frac{1}{2}\varphi^2, \text{ L=2.4x10}^{-8} \text{ (V/K)}^2 . \quad (2.15)$$

For a long constriction voltage with the total voltage V and the room temperature T_0, we can obtain the following equation.

$$L(T_\theta^2 - T_0^2) = \frac{V^2}{4} \quad (2.16)$$

The constriction voltage arises from two points which are the meeting point of the bulk and the constriction. That is why a half of total voltage is put into the equation.

Though this equation shows the relation of the voltage and temperature, it is a simple case. This equation is induced in the condition that the electrical resistivity and thermal conductivity is constant regardless of the elevating temperature due to joule heating. Actually, they have dependence on the temperature. Furthermore, the

contact area is expended when the temperature is elevated. In really, such deviation from theory is reported in the some references. However, our concern is that the melting phenomenon in the contact, not the exact voltage value. Thus, the above simple equation is enough to explain our experimental data.

2.4 Resistance change from High resistance to Low resistance

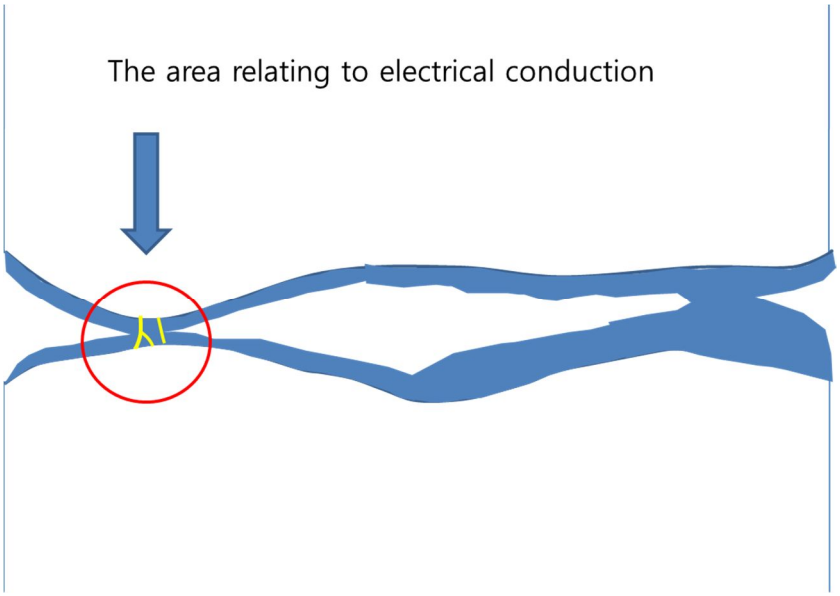

Figure 2.8 | The occurrence of conducting filaments in the interface. It is possible that the MIM structures lose their insulation by high electric field. In that case, the electrical resistance of the structures is lowered severely.

The electrical resistance of contact is dependent on the metal-metal contact area size formed when two contact members are met. But, generally the contact surface is covered with a thin oxide layer, even if the material for protection against it, like stainless steel [51]. In that case, the electrical resistance of the contact is very high, it is enough to cause trouble in the electronic circuit.

The method to make a low resistance contact is a big load applying to the contact. Then, some high asperities on the one surface are faced at the other contact surface, directly. Thus, the surface parameter like roughness and material parameter like Young's modulus, yield strength [30, 32]. However, the oxide layer on the surface is not destroyed in the case of the very low contact load. Then, the transition from a high resistance contact state to a low one can occur through the electrical impact [38, 40]. Usually, this transition is called by dielectric breakdown, which have been studied since tens of years ago [71-79].

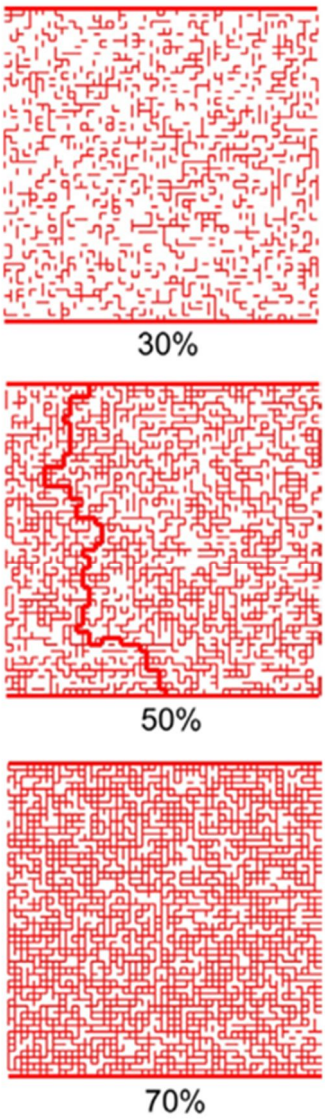

Figure 2.9 | Examples of bond percolation [80, 81]. The long path connecting between two sides can be formed when the concentration of conducting material is larger than a specific value.

The transition is considered as the formation of conducting paths inside the oxide layer. This filament-like conducting path can be modeled by a dynamic percolation model [80]. In static percolation theory, the occurrence of one dot at each site is dependent on the initial probability [81, 82]. If initial probability is larger than a certain value, which calls percolation threshold and it is different by lattice, the infinite cluster which crosses from one end to the other end of the system is formed. This is inappropriate to the dielectric breakdown modeling. In dielectric breakdown phenomena, the forming of the conducting dot is dependent on local electric field. Thus, in dynamic percolation model the occurrence probability is dependent on the local field [41-43, 83-85].

An oxide layer is modeled by resistor network where each resistor has a high resistance. And in the network, a low resistance resistor, which is considered as a defect inside the oxide layer, is randomly distributed with a certain probability. We treat the pristine oxide layer with this random resistor network. Then, the rest work is to repeat the calculation of local electric field at each resistor and the rebuild of network by its result until the whole reaches convergence.

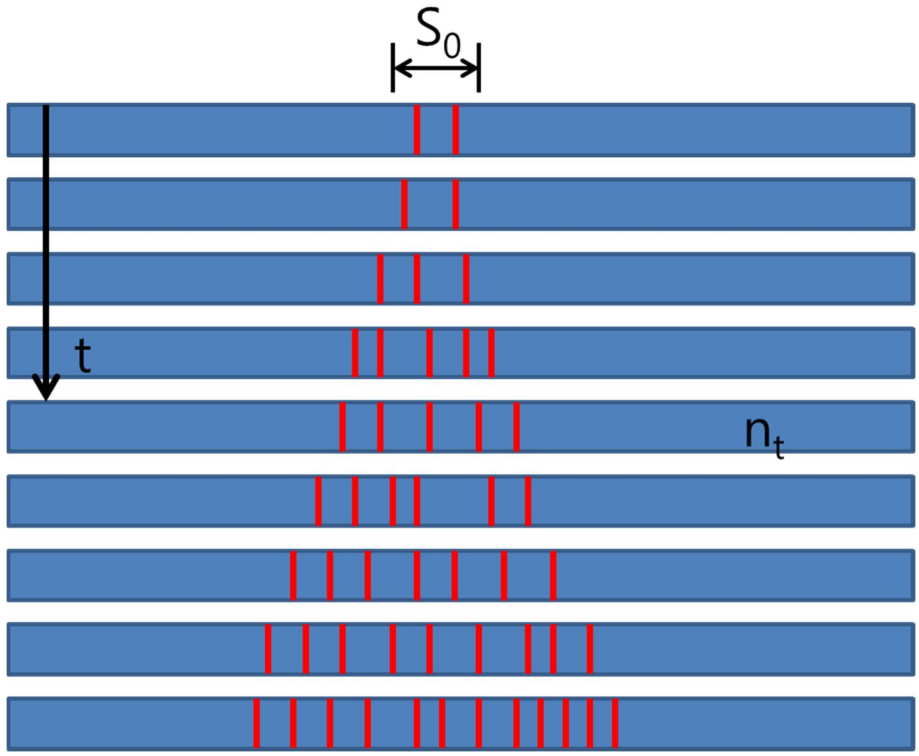

Figure 2.10 | Forming the filament in two dimensional stacked layer model [80]. This figure shows the idea of filaments bundle in the insulating layer.

In rough calculation, we can obtain the relation between the total resistance of network and lateral size where dielectric breakdown occur. Assuming that the oxide layer is considered two dimensional stacked sheets, we can cut the filaments by sheet. Numbering from top sheet, the depth t is represented by number from top electrode and the filament pieces on the sheet number t, n_t, means the number of the conducting bond at depth t. In that case, the total resistance of filaments, R_0, is

represented by

$$R_0 = r\sum_k \left(\frac{i_k}{I_{tot}}\right)^2, \tag{2.17}$$

where k denotes the conducting bond, I_{tot} is the total current, which is from external source, passing the network, the r is the constant determined by material, which is each resistance of bond. If we assumed that the current passed by each bond on the same depth is same, $i_1 \approx i_2 \approx \cdots \approx i_t \approx \frac{I_{tot}}{n_t}$,

then,

$$R_0 \propto \sum_{t=0} \left(\frac{1}{n_t}\right)^2 n_t. \tag{2.18}$$

By scaling relations of three dimensional conducting paths, the approximation, $n_t \sim (s_0 + t)^{D_f - 1}$where s_0 is the lateral size of the bottleneck and D_f is the fractal dimension of conducing paths, is obtained[21]. This approximation is substituted to above equation,

$$R_0 \propto \sum_{t=0} \frac{1}{(s_0+t)^{D_f-1}}. \tag{2.19}$$

In the regime of very small s_0, the dominant term of the above summation is the first term of it, then $R_0 \sim \frac{1}{{S_0}^{D_f-1}}$. And the above summation satisfies the limit relation, $\int_0^N \frac{dt}{(S_0+t)^{D_f-1}} < R_0 < \int_0^N \frac{dt}{(S_0+t)^{D_f-1}} + \frac{1}{{s_0}^{D_f-1}}$, then in the regime of sufficiently large s_0, the approximation resistance is $R_0 \sim \int_0^N \frac{dt}{(S_0+t)^{D_f-1}} \sim \frac{1}{{S_0}^{D_f-2}}$. Thus, we obtain the two relations of the conduction paths formed by dielectric breakdown by s_0 and D_f.

$$R_0 \sim \begin{cases} {s_0}^{-D_f+1} \text{ for small } s_0 \\ {s_0}^{-D_f+2} \text{ for large } s_0 \end{cases} \tag{2.20}$$

This means that the resistance of the conduction paths formed by dielectric breakdown is dependent on the lateral size of the bottleneck site which dielectric breakdown occurs and the fractal dimension of the conduction paths. Thus, the fluctuation of it can be seen by the sum both one fluctuation with one mean value and another fluctuation with another mean values.

2.5 log-normal distribution of filaments' resistance

The log-normal distribution of the resistance of a conduction path has been explained by the hopping model used in resistive switching phenomena; the conduction path is described as a series of defects, like stepping stones.

$$P \sim \exp\left[-2\alpha R - \frac{W}{kT}\right] \tag{2.21}$$

P is the hopping probability of two states, which can represent the current. R, W are the special separation, the energy difference of two states, respectively. α^{-1} is the attenuation length of hydrogen – like localized wave function, and k, T are Boltzmann constant and temperature. This shows that the hopping current have an exponential dependence on the spatial separation of two states [86-88].

The fluctuation in the resistance of a conducting path has been reported to occur as the result of deviations in the separation between the defects. However, it is difficult to explain the results of our study with the hopping model because the difference between the high and low resistance in our results is much larger than that observed in resistive switching. Furthermore, the conduction path modeled by the hopping model is 1-d line-like path, but the fact that the path formed by electric breakdown is a tree-shaped filament with a specific fractal dimension has been reported.

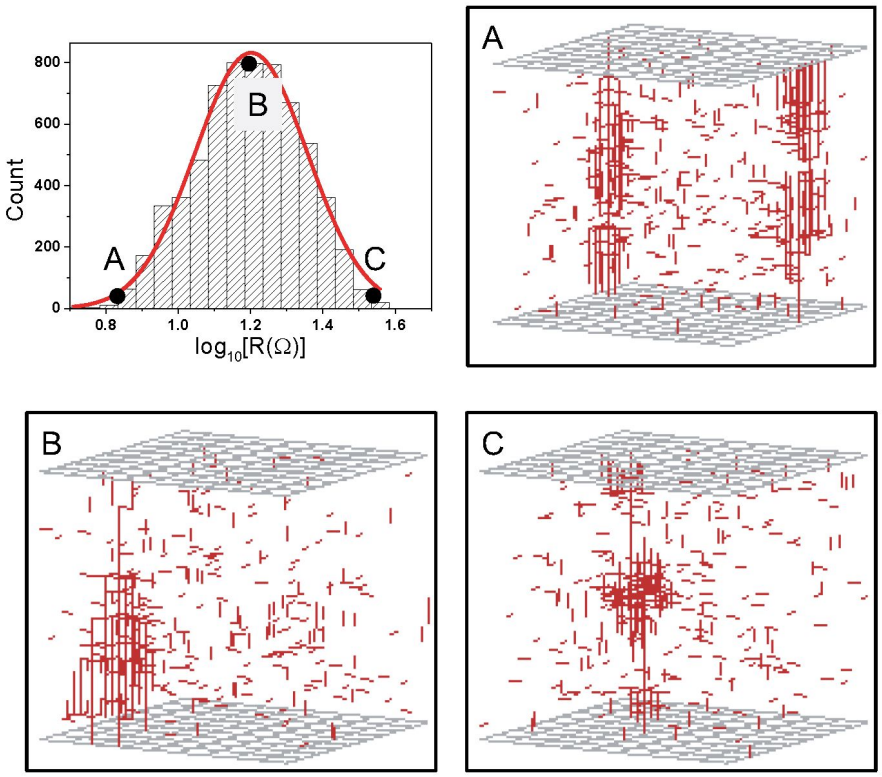

Figure 2.11 | The log normal distribution of filament bundle's resistance. The origin of the log normal distribution is the asymmetry frequency of filament bundle and the wide range of filament bundle's resistance

Alternatively, we could explain the electrical conduction behavior for the low contact resistance by the random circuit breaker (RCB) network model, which has explained the resistive switching phenomenon in thin oxide films through the formation/rupture of nanoscaled filaments. The simulation results using this model

show a log-normal distribution for the resistance of filamentary conducting paths. Different from the hopping model, which considers the random variable to be the separation between defects in an insulating layer, the random variable in the RCB network model is the initial position of defects inside the insulating layer. Thus, it is difficult to explain the origin of the log-normal distribution as simply as in the hopping model. To find the origin of the log-normal distribution, we examined the configuration of several filaments. There are three representative types of conducting filaments for the low contact resistance, as shown in Fig. 2.10: the first involves multiple filaments with a resistance of several Ω; the second is a tree-shaped single filament with many branches contacting the electrode at a resistance of 10 - 30 Ω; the third is a line-shaped single filament with few branches extending towards the electrode at a resistance of 50 - 100 Ω. Of course there are residual high resistance values between two bimodal distributions. However, because these values should have different bond transport mechanism from diffusive motion and they are of rare occurrence, we neglected them in our simulation.

As a matter of course, these types of filaments have different occurrence probabilities. The major type of filament is the tree-like structure with a resistance that substantially depends on the shape of branches percolating toward the electrode. The least probable type of filament is the line-like structure in which the initiator of the filament is isolated and not merged during growth with other branches grown from other sites on the electrodes. Because the initiators of a filament on the electrode must be widely separated from each other, multiple filaments are also uncommon; thus, the log-normal distribution for the resistance of the conducting path is a reflection of the asymmetric occurrence of diverse growth patterns of filaments inside the insulating layer and the wide range of the tree-like filaments' resistance.

Chapter 3

Experiment setup and method

3.1 Properties of Type 304 stainless steel

	Signification	Value
ν	Poisson's ratio	0.27
E	Young's modulus	1.95 X 10^{11} N/m^2
ρ_{el}	Electrical resistivity 20 ℃	72 μΩ cm
	650 ℃	116 μΩ cm
λ	Thermal conductivity 20 ℃	16.2 W/(km)
	500 ℃	21.5 W/(km)
T_{mel}	Approx. melting point	1425 ℃

Table 3.1 | Mechanical, Electrical, and Thermal Property of Type 304 stainless steel [89].

Two identical stainless steel (AISI/SAE type 304) ball with diameter 0.95 cm and mass 3.58 g are used. Table 3.1 is the electrical, thermal, and mechanical properties of Type 304 stainless steel. Its mechanical property is need for calculating the apparent contact area size when two balls are met with the contact load corresponding to its weight. Thermal property is for getting approximation of melting voltage. Aforementioned, the reason of using stainless steel ball is its mechanical robustness and inoxidizable surface.

3.2 Experimental setup

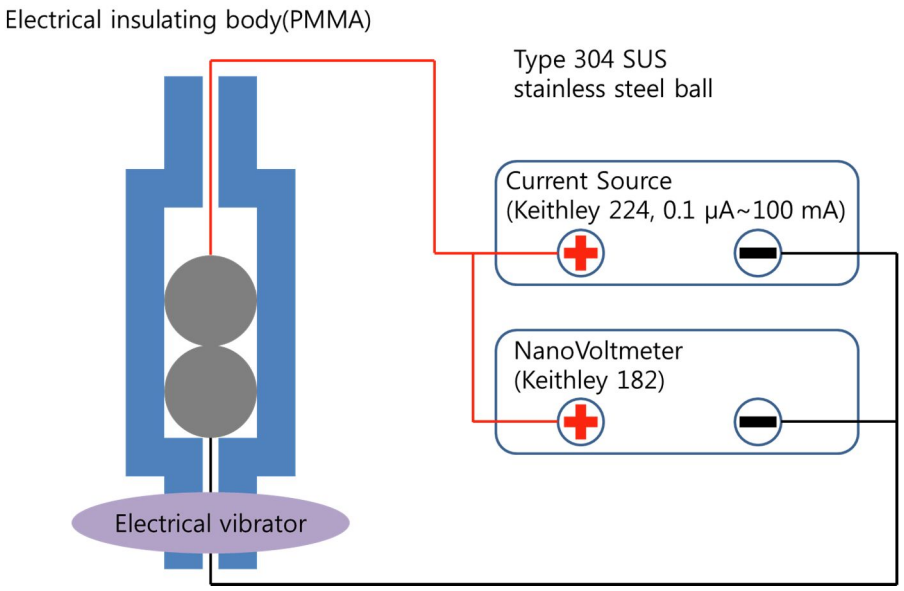

Figure 3.1 | Experiment setup.

The experimental setup is shown in Figure 3.1. The structure confining the stacked ball array is a plastic cylinder (polymethyl methacrylate, PMMA) with a diameter of 3 cm and a length of 10 cm. The cylinder is hollow and fits the balls snugly (Diameter of the hollow is larger than that of the balls by 5%). An electric vibrator to perturb the balls mechanically is attached to the bottom of the cylinder. A thin copper wire (0.08 mm diameter) is soldered to the upper ball, and a thicker wire is soldered to the lower ball. A dc current flows from a current source (Keithley Model 224) to the ball array, and the voltage across the balls is measured by a nanovoltmeter (Keithley Model 182). The current source can supply constant currents in the range from 0.1 μA to 100 mA, and the output voltage limit can be set in the range from 1 V to 100 V. The nanovoltmeter measures dc voltages up to 30 V with a maximum resolution 1 nV. During the experiment, we supplied a constant current (0.1 μA and 1 μA) and measured the voltage to determine the contact resistances.

3.3 Experimental method

3.3.1 Distribution of electrical contact resistance

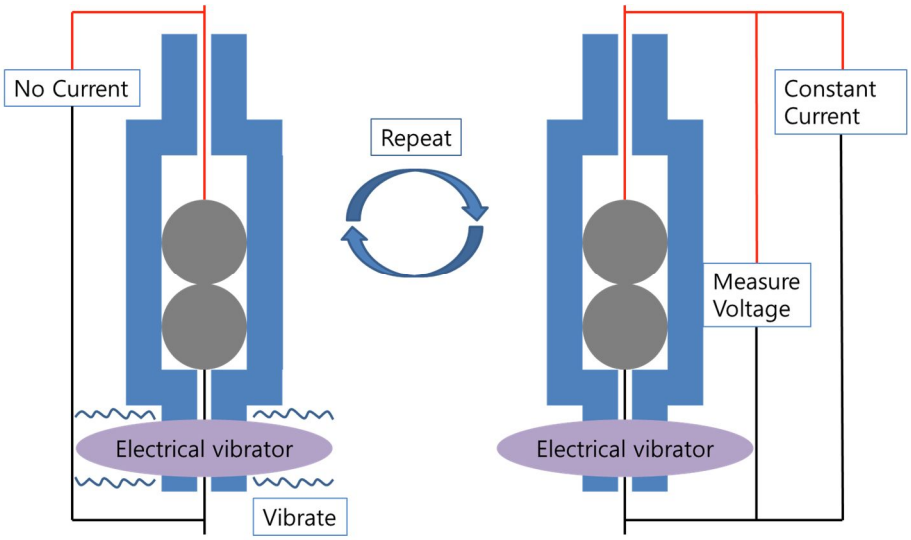

Figure 3.2 | The set up of Measuring the distribution of electrical contact resistance. This is for repeating many measurements.

At first, we vibrate the system using electrical vibrator during 0.08s. In this time, the body move from side to side and its movement is about 400 μm. Then, we wait during 3.5s, it is for stabilizing the system and preventing the measurement from being disturbing because of earlier vibration. And the current for measure flows on the contact, while we measure the voltage of the contact at that current. Thereafter, the current turn off. The total time of one measurement is 10 seconds. We repeat this process to set number.

3.3.2 I-V measurements

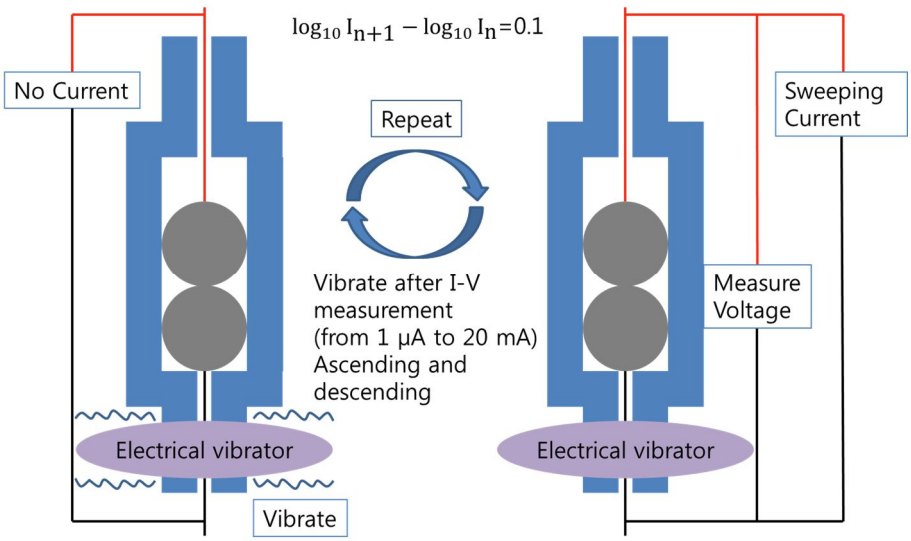

Figure 3.3 | The I-V measurements of electrical contact resistance. The wide range of current is for observing a sudden drop of voltage in the contact

The method making a new contact state is same with former method. In this experiment, we measure voltage with increasing current. For getting the data in very wide range of current, the current increases exponentially. The multiple step between two sequential current applying to contact is $10^{0.1}$ times. The range of current is from 1 μA to 20 mA, and the current source (Keithley model 263) is used. At first, we measure the voltage of the contact at each current for direction of

ascending, and reaching 20 mA, we measure it for direction of descending. The total time of one I-V measurement is 190 seconds, and the point is 70. We repeated this process to set number, for statistical study of I-V graph.

3.4 Simulation

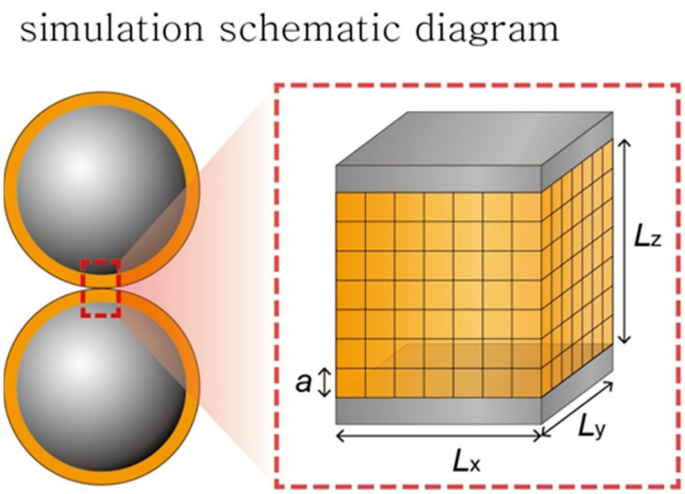

Figure 3.4 | Schematic diagram of simulation. Each edge is 20-lattice and the length of it is assumed by 0.3 nm.

Figure 3.4 is the simulation schematic diagram. The insulating film between contact

members is realized by cubic with the edge of 20-lattice, and the lattice constant is assumed by 0.3 nm. The resistance of the bond connecting two adjacent lattice points is one of 1.5 Ω or 0.6 MΩ. The bond with 1.5 Ω is an original defect in the oxide layer, also it can be made when the local electric field to a high resistance bond is larger than a threshold values, which is 100 MV/m in our simulation. The simulation is carried out at constant current mode.

At beginning of simulation, we give the cubic 1.1% defects, randomly. And we repeat calculating a local electric field of each bond and changing the high resistance bond with larger value than threshold value into the low resistance bond, as the voltage increases by a fixed step. The total current of the network is also calculated at each step, and the simulation is over when it reaches set current. In this case, the set current is 11 μA.

Chapter 4

Experiment result and discussion

4.1 The distribution of electrical contact resistance

The electrical contact resistance has been study since 1960s. Almost results about the electrical contact resistance confirm the theory of Holm and Sharvin. We expected that our experiment result was also included into those categories. Our original purpose was the examination of what the electrical property of the resistor network, like a conducting granular system, is. For this purpose, we examined the electrical property of a single contact, then we anticipated the comprehensive understand of the total network system that was composed of many contacts, on the result of one contact.

4.1.1 Two kinds of electric contact resistance

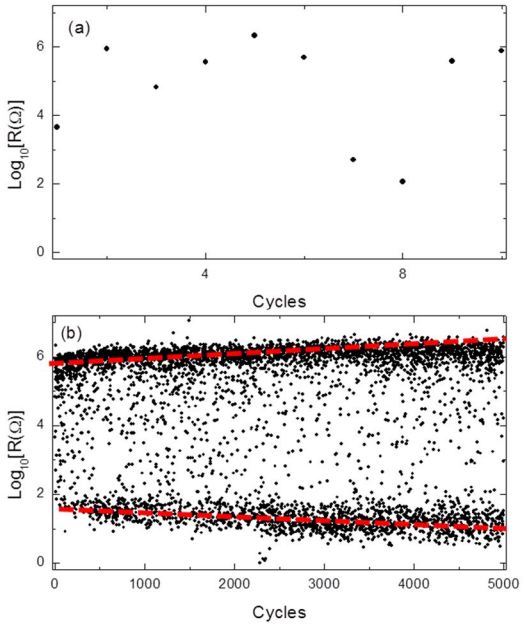

Figure 4.1 | Electrical contact resistance at current 1 μA. There two electrical states in a weak contact: one is a low resistance contact, another is a high resistance contact.

In the beginning of the experiment, we expected that the electrical contact resistance in a single contact is distributed normally. The load applying to the contact is a constant with some fluctuation coming from the friction or lean against the wall of the body. The contact load is related to the contact area size. In that case, the small fluctuation of a load to the contact gives rise to that of the contact area size. And, in general, the natural fluctuation is a normal distribution. If the electrical contact, which is called by α-spots in the field of electrical contact field, is formed by

mechanical parameters, then the result will be obtained according to our expectation.

Figure 4.1 is the statistical result of the electrical contact resistance in a single contact, where the current is 1 μA. Figure 4.1(a) is the 10 measurements of the electrical contact resistance. It shows that the electrical contact resistance appearing in our sample varies widely. Thus, we cannot get the tendency of the distribution as well as the mean value of a contact resistance, in the small number of measurements. For getting such data, we performed many repetitions of same procedure. As a result, we knew that our expectation about the resistance of a single contact must be modified.

In the result of many measurements, the electrical contact resistance is divided into two categories, as shown in the figure 4.1(b): one is the contact with low resistance, another is the contact with high resistance. For the more distinct view about the distribution of the contact resistance, we need a secondary data of figure 4.1(b).

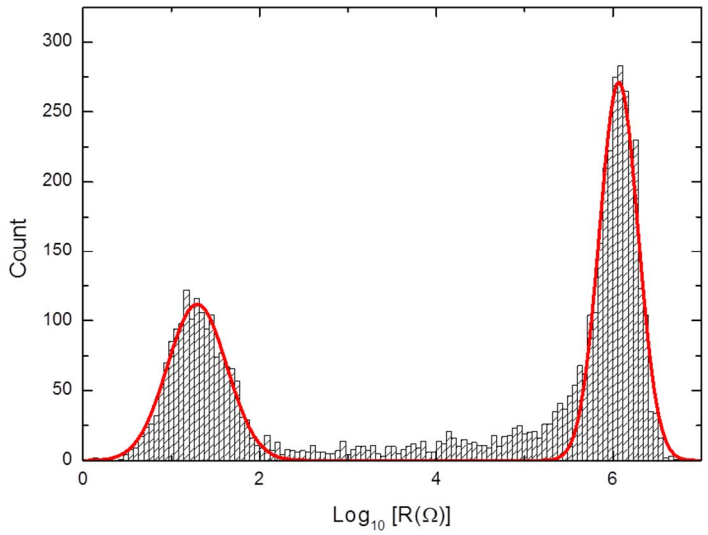

Figure 4.2 | Histogram of electrical contact resistance at current 1 μA. The mean value of low resistance is about 20 Ω and that of high resistance is about 1MΩ.

Figure 4.2 is the histogram of the data in the figure 4.1(b). The histogram in Figure 2(b) shows the presence of two peaks in the $\log_{10}[R(\Omega)]$ distribution. Furthermore, the distributions around the two peaks have nearly normal distributions and can be fitted as a normal distribution. The red line in this figure is the fitting line of Gaussian function with two peaks. The mean value of a low resistance peak in that line is 1.29 (～ 20 Ω) with standard deviation of 0.4, and the mean value of a high resistance peak in that line is 6.07 (～ 1.2 MΩ) with standard deviation of 0.26.

Additionally, one point is worth mentioning from the data in figure 4.1(b). Small drifts occur in the major parts of the data in figure 4.1(b) as the repetition of measurement sequence proceeds. The higher resistance peak shifts to higher resistance values, and the lower resistance peak moves to lower resistance values. This shift may indicate changes in the contact region due to the continued application of vibration to the balls, and it is well-known phenomenon that is named by fretting in the field of electrical contact. Though we used a stainless steel ball for preventing this change by mechanical or electrical factors, it is impossible to be blocked perfectly. However, these drifts usually slow down after first thousand times measurements. The major characteristics of distribution do not change as the measurements proceed. If we extract enough number of data in the figure 4.1(b) and make a histogram, the shape of its distribution is not varied, even if its mean value is changed a little.

4.1.2 The origin of a low and high resistance contact

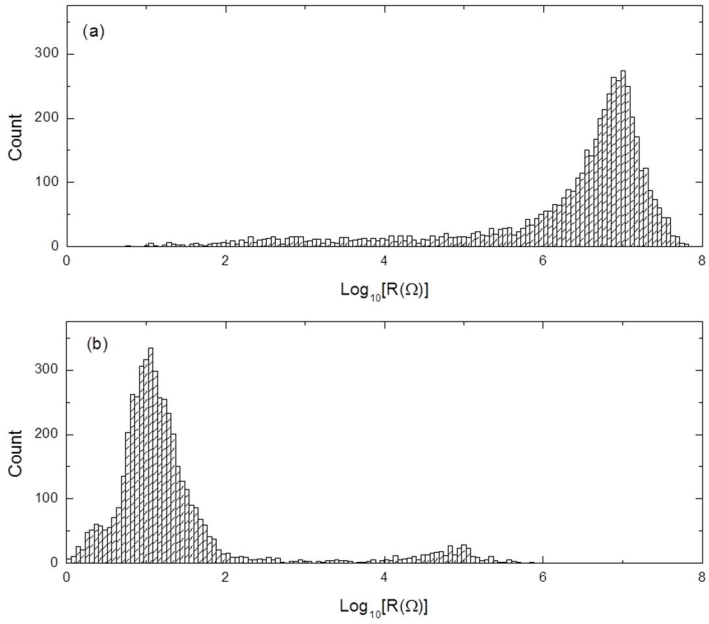

Figure 4.3 | Distribution of electrical contact resistance at current (a) 0.1 μA and (b) 10 μA. At low current, there are few low resistance contact, while the high resistance contact is disappeared with increasing current.

We think that this unexpected result is due to ignoring a thin oxide layer on the surface. Identifying our new idea, we adjust the current on the contact. Figure 4.3 is the result of (a) 0.1μA and (b) 10 μA. As shown in the figure 4.3, the distribution of the contact resistance varies dependent on the current on the contact. In conjunction with figure 4.2, it looks like a transition from a high resistance contact to a low resistance contact by current increase. There are almost high resistance states at low current, and as the current on the contact increase, more low resistance states occurs.

That is, the contact state with low resistance made by electrical parameters, not mechanical ones, which are expected by the origin of forming an electrical contact.

Additionally, we examined the oxide layer thickness using XPS depth profile data for more insight. The ball's XPS experiment is impossible because it is not fixed in the sample chamber as well as entered because of its big size. Thus, we bought the flat plate made by the same material with our stainless steel ball. For depth profile, the Ar sputtering is needed. The procedure is repeating Ar sputtering and XPS measurement. But, because the stainless steel is an alloy, we cannot identify the sputtering rate per minute, exactly. We obtain approximate value referencing to the sputtering rate of the ingredients of a Type 304 stainless steel. It is roughly 5 to 10 Å per minute.

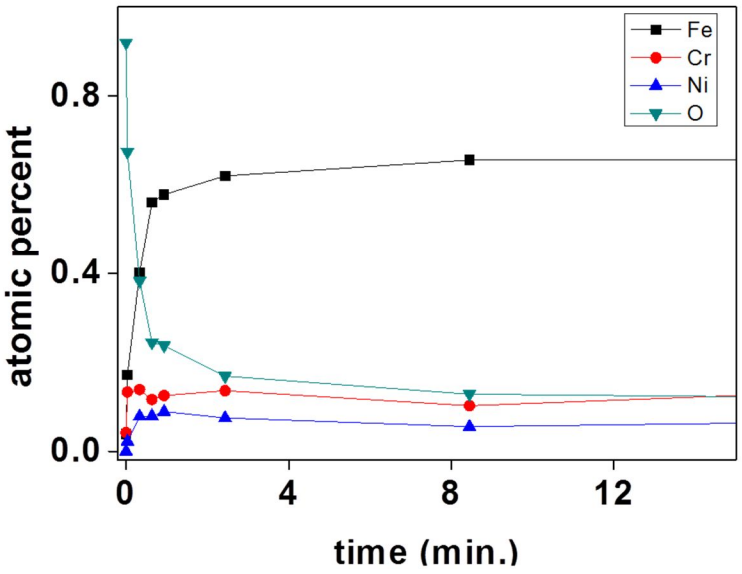

Figure 4.4 | XPS depth profile of usual Type 304 stainless steel plate. This shows that there is a few nanometers-thick oxide layer on the stainless steel surface.

Figure 4.4 is the result of XPS data analysis. The used stainless steel is mainly comprised of Fe, Cr, Ni with a very small percentage of Mn. The ratio of each ingredient in the Type 304 stainless steel is Cr 18%, Ni 10%, and Fe is almost balanced. Our main concern is the oxide percentage with respect to the depth from the surface. In the figure 4.4, the percentage of an oxide decreases exponentially with increasing depth. The definition of the oxide layer thickness is very difficult with this figure. However, we define it as 2.5 nm to 5 nm. It is the conversion of time to depth at the sixth point of symbol representing the oxygen. It is very rough

value. But, its exact value is not important for us because the important point to us is the existence of the oxide layer with several nanometers thick on the surface. That is enough to support our new idea.

4.2 Time evolution of electrical contact resistance

The electrical resistance of the contact separating by a thin oxide layer is changed with time evolution. The electrical contact resistance shows two aspects with respect to time evolution: one is a slow variation like slow relaxation shown in the granular matter and another is a sudden change shown in the dielectric breakdown phenomenon. Specially, the slow change of the electrical contact resistance is another result against our expectation. We considered the slow relaxation as the particular property of granular system.

4.2.1 Slow change of electrical contact resistance

Figure 4.5 is two representatives of a contact resistance slow change with respect to time. The current in the contact was 1 μA and the measurement was performed during 1000 seconds. Figure 4.5(a) is the case of a high resistance contact and

figure 4.5(b) is the case of a low one. Though the electrical contact resistance does not always fall down with time evolution, most cases shows the tendency of the falling resistance. And, the variation of the resistance in a high resistance contact is larger than that in a low resistance contact.

As shown in the figure 4.5, the change of electrical resistance with the time evolution is different from each other with respect to the resistance value. The relative variation, which is defined by the ration of the difference between initial and final resistance to initial resistance, is about 0.5% in the low resistance contact and 20% in the high resistance contact. This means the origin of the contact resistance with two regimes, which are a high resistance state and a low one, is different from each other, indirectly.

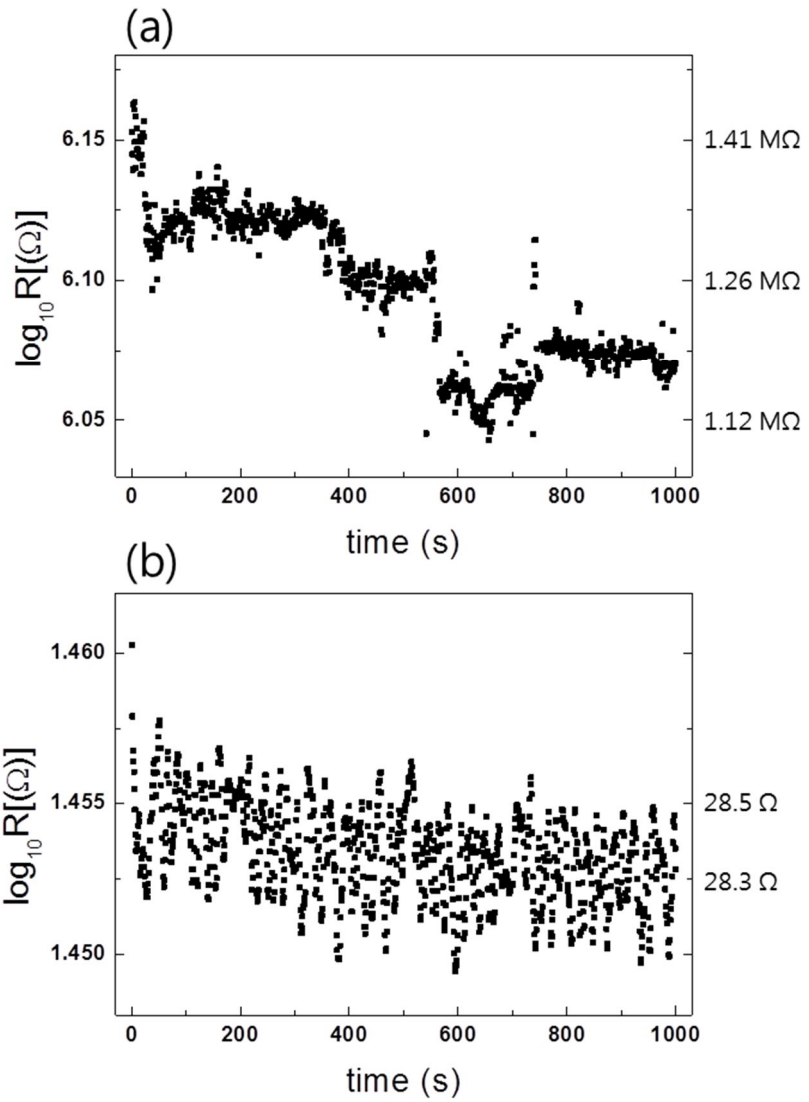

Figure 4.5 |Time evolution of contact resistance. According to initial resistance, the ratio of variation is different. The high resistance contact varies more than the low resistance contact.

4.2.2 A sudden drop of electrical resistance

Figure 4.6 is two representatives of the sudden change of contact resistance in a certain time. Figure 4.6(a) shows two types of changes in the severity of change. These types of resistance change are appeared in the MOS (Metal-Oxide-Semiconductor) breakdown phenomena. The small change is called by the soft dielectric breakdown (SBD) and the large change is called by the hard dielectric breakdown (HBD). And this phenomenon, which is that an abrupt change of the resistance in the system occurs at a certain time, is called by time dependent dielectric breakdown (TDDB).

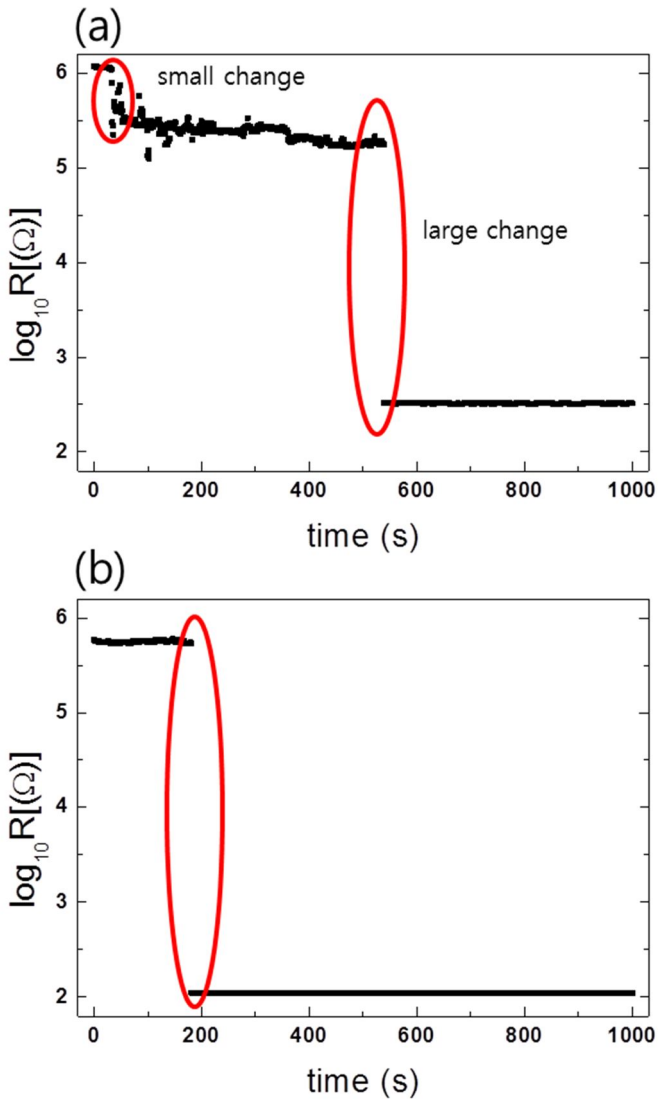

Figure 4.6 | A sudden change of electrical contact resistance. There are two types: a small change and a large change. But, they are a relative concept each other.

To examine the origin of the slow change in the contact resistance, we repeat time evolution experiment with same condition, except for two conditions. They are mechanical load and the electrical sourcing time on the contact.

In the high resistance contact, we think the reason of the slow change as the slow change of the distance of the nearest site between contact members with time evolution, and it is reasonable that the separation between two contact members is closer because of the weight of the upper ball. But, at first, we doubted the electrical migration or move of defect in the anode or cathode by electrical force. Because, the effect of electrical factor is higher than that of mechanical factor, even if the current is only for measuring the electrical contact resistance. Thus, we flew the current in the contact, intermittently. The interval of the current applied to the contact was one second per fifty seconds. However, the difference is not clear as we expected.

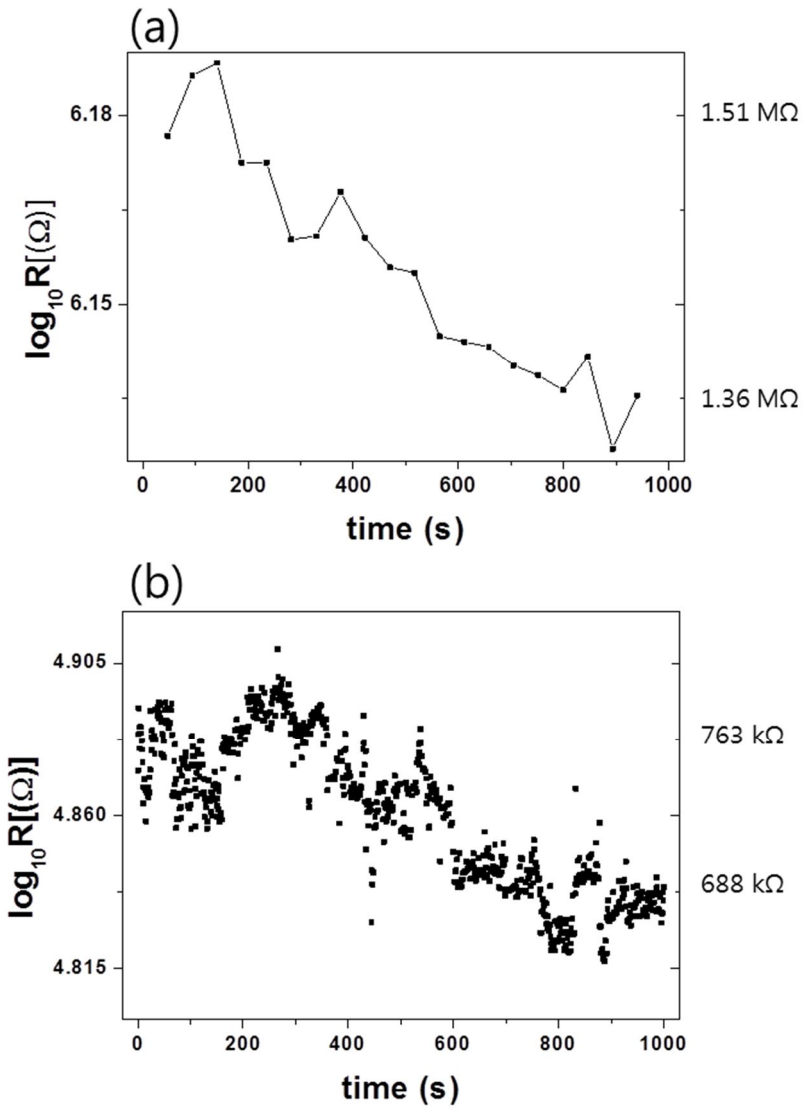

Figure 4.7 | the variation of electrical contact resistance with respect to intermittent current and the higher contact load.

For the second time, we examined the effect of the mechanical factor that is the depression of the oxide layer by the mechanical load. Figure 4.7(b) is the result of the same experiment with figure 4.5(a), except for the mechanical load applied to the contact. The contact load is about five times that in the case of figure 4.5(a), which is formed by putting four balls on the upper ball. Comparing that in the fig. 4.5(a), the initial resistance is reduced on the one or two order scale. But, the distinct difference in the view of its resistance change is not appeared comparing with fig. 4.5(a).

4.3 I-V characteristic

For obtaining more information about electrical property, we measure the voltage with increasing current gradually. The increasing multiple between before and after the current is $10^{0.1}$ because of its wide range from 1μA to 20 mA. Through this I – V measurement, we identified the characteristic of the electrical contact by its resistance value, which was related to the origin which the electrical contact comes from.

4.3.1 The diverse I - V characteristics

Figure 4.8 is an assortment of fifty I-V measurements and five representatives of diverse I-V graphs. The graphs in the Figure 4.8(b) is the cases where a drastic voltage change in the contact does not occur, while the graphs shown in the figure 4.8(c) is the other cases where a drastic voltage drop exists.

Fig. 4.8(a) shows a diversity of I – V characteristics. However, these I – V characteristics can be divided by its initial resistance. Below the 10 kΩ which is the point of 10^{-2} V and 10^{-6} A, the I – V characteristic shows a linearity, otherwise they shows non-linearity. The reason of appearing a linear I – V characteristic in the contact separating by a thin oxide layer is for a conducting path to be formed connecting two contact members. This is supported by the fact that the resistance corresponding to quantum conductance is 12.9 kΩ.

The graph of the number 1 in the figure 4.8(b) shows this saturation like aspect, more clearly, even if the initial aspect is different from each other. And the number 3 graph shows the characteristic of a resistor with Ohmic one. We think the difference of initial aspect between 1 and 2 is reflection of the contact state, which is the configuration or number of the conducting path inside the insulating layer. That the voltage dose not proceed 0.4 V is the reflection of joule heating in the contact.

Three representatives in the figure 4.8(c) are the I-V graphs where the dielectric breakdown occurs. The symbol graph numbered by 3 in the fig. 4.8(c) shows the slow increase of the contact voltage with increasing current, then the voltage falls down at a certain high current and it holds at that voltage, as seen in the saturating phenomenon. And, a drastic voltage drop is appeared in the other cases. The difference between two graphs is the initial aspect. One is Ohmic

characteristic, another is non-Ohmic characteristic. We think that these two characteristics are reflection of whether a thin oxide layer in the interface exists or not. However, the interesting point in this figure is that it is possible for a dielectric breakdown to occur in the contact where the metal-metal bridge is formed. This means that even if the metal bridge between contact members is formed, another bridge can be formed in another site.

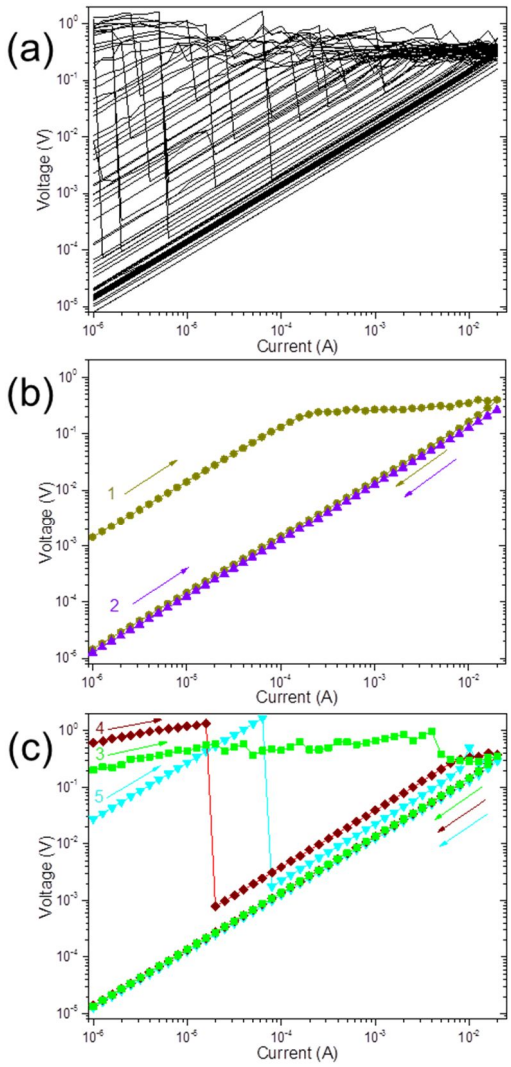

Figure 4.8 | Fifty I-V measurements and five representatives of I-V measurements. These graph shows diverse I-V characteristics of electrical contacts and a sudden drop of voltage in the contact.

Additionally, we can identify the difference between melting phenomenon and dielectric breakdown in the I-V graph. The dielectric breakdown is an instant point in the I-V graph, while the melting phenomenon is a continuous state in the I-V graph. A dielectric breakdown is the forming current paths in the interface and it is like a resistor with Ohmic characteristic, while melting is the phenomenon after the metal-metal contact is made and the contact resistance is decreasing with increasing current because of joule heating in the contact.

4.3.2 The dielectric breakdown voltage and its severity

For establishing what the electrical factor causing a dielectric breakdown in the contact is, we make a histogram about the current, voltage, power of points where a drastic voltage drops in the I-V graph. Point getting the data is determined by the point being 10-fold larger than the following point. In other word, when the ratio between two sequential points in the I-V measurement is more than 10-fold, the before point is the point to get the data about a dielectric breakdown.

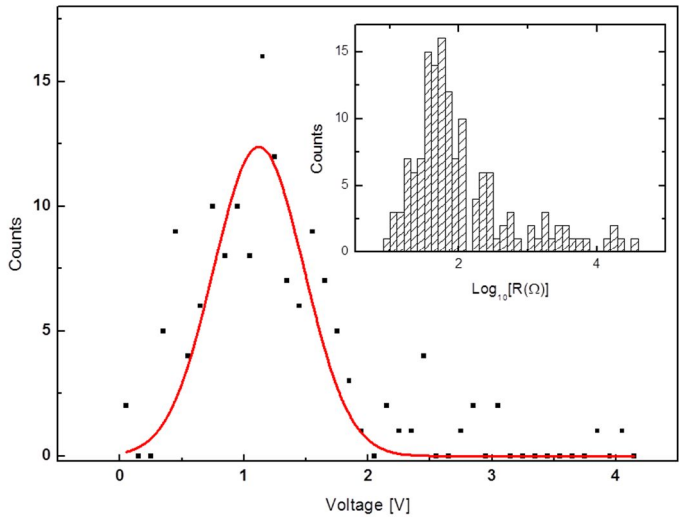

Figure 4.9 | The distribution of breakdown voltage and contact resistance after breakdown. This shows that the mean voltage at a sudden drop is 1.1 V and it is similar to the resistance distribution of a low resistance contact.

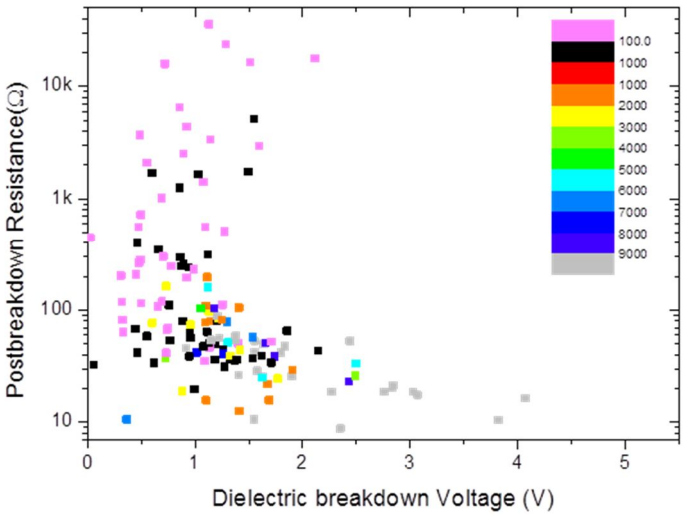

Figure 4.10 | The severity of dielectric breakdown and post-breakdown resistance. As the voltage is bigger, the severity is also bigger.

Figure 4.9 is the distribution of the voltage of points determined by above paragraph. We get also the distribution of the power and current of those points, but we cannot get any inspiration about the distribution. On the contrary, the voltage histogram shows some distribution, which is a normal distribution. The normal distribution is a universal distribution in the nature. Thus, we think the factor causing a dielectric breakdown of the voltage between contact members, and more strictly speaking, the electric field is.

The inset in the figure 4.9 is the distribution of the resistance at the breakdown

point determined in the above paragraph. This is very similar to the distribution of the low resistance part in the figure 4.2. This inset shows a log-normal distribution with long tail toward high resistance part. We considered this long tail toward high resistance part as the contact is broken partially or a very thin conducting path is created. They are rare events, comparing to the occurrence of the contact broken severely or the thicker conducting path.

Figure 4.10 shows the relation of dielectric breakdown voltage and post – breakdown resistance. As we expect, the higher dielectric breakdown voltage is, the lower post – breakdown resistance is. And the severity increases with increase of dielectric breakdown voltage. But, the range of post – breakdown resistance is very wide when the dielectric breakdown occurs at the low voltage, the severity is not large. These lead two results: one is that the dielectric breakdown can occur in any contact states which are both a low resistance contact and a high resistance contact, another is that the post – breakdown resistance is less than 10 kΩ, in consistent with quantum conductance theory. Furthermore, this figure reminds us that the determination of dielectric breakdown voltage must be careful.

4.3.3 The distribution of electrical resistance after melting

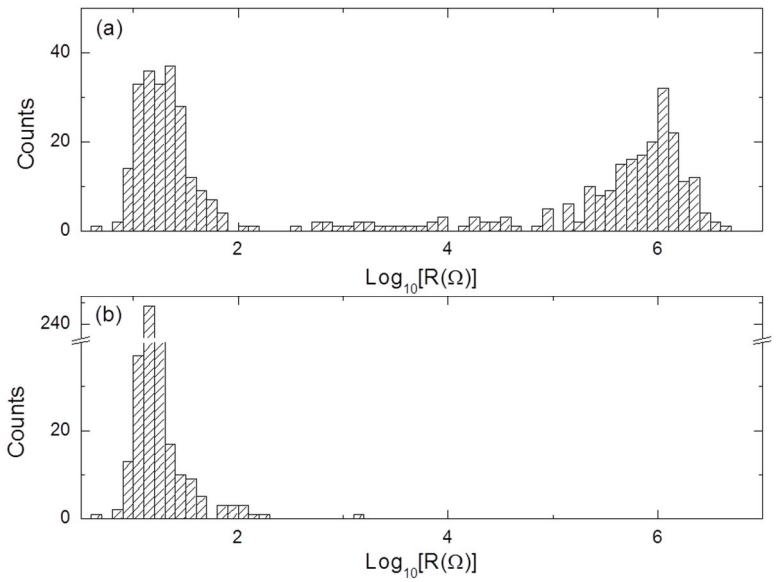

Figure 4.11 | The distribution of initial and final electrical contact resistance of I-V measurement. This shows the difference of two distributions which are the dielectric breakdown and melting cases

Figure 4.11 is the distribution of the (a) initial and (b) final contact resistance in the I-V measurement. The distribution of initial resistance is same with the figure 4.2, and it is reasonable. And Figure 2 is the distribution of the contact resistance after melting occurs in the contact. The melting voltage is well known in the contact theory. The metal-metal contact is heated by joule energy, then, its temperature can be elevated at the melting point of metal. Thus, the melting voltage is different from each material, but its range is not wide. In almost conduction metal, it is less than 1

V. Because the stainless steel is alloy, the melting voltage of it is that of the ingredient, and we suppose it by Fe, whose melting voltage is about 0.43 V. We note that the melting occurs after the conducting path is created. That is well shown in the many I – V graphs.

4.4 Dependence on current

The resistance arising from the oxide layer is varied by the external source level, which can be expected from the Simon's J-V relation. In low level, the resistance of it is independent on the external source level, but in high level, the resistance of it is dependent on the external source level.

Figure 4.12 is the distribution of the electrical contact resistance with increasing current. There exist two peaks in the each current, except for the case of the current 0.1 μA. And, Fig. 4.12 shows that the mean value of low resistance in each distribution hold with increasing current, while that of high resistance move toward the low resistance. This means that the high resistance arising from contact is due to the existence of a thin oxide layer. That is tunneling resistance. If the oxide layer between two contact members is thicker, the current cannot flow through the oxide layer. On the contrary, if there does not exist an oxide layer between two members, the resistance is fixed regardless of the current, as the low resistance peak in the fig. 4.12.

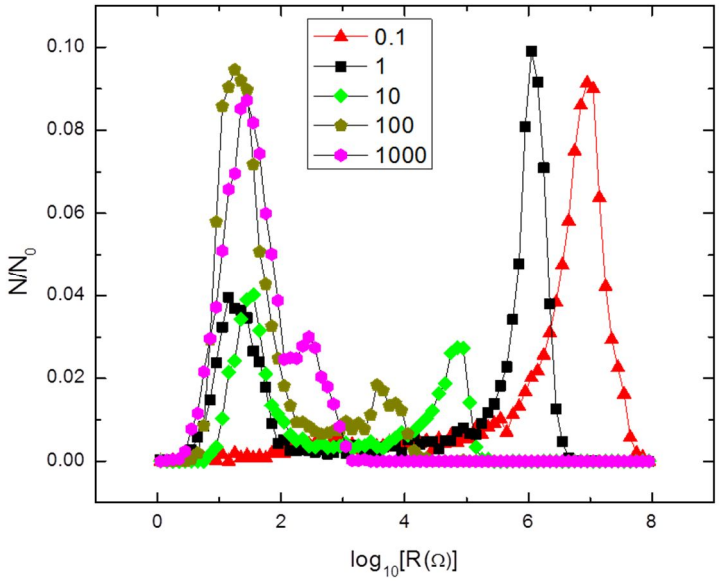

Figure 4.12 | The variation of the resistance distribution with respect to current. As the current is higher, the frequency of a high resistance contact is reduced and the mean value of a high resistance moves toward low resistance

In addition, the occurrence probability of a low resistance contact increase with increasing current. This means the increase of the probability which is that of forming the conducting filament inside the oxide layer. For applying high current to the contact, the voltage to the contact can be higher. Though an oxide layer between

the contact members can withdraw the high voltage, the probability of making such contact in the initial state is much lower, as the current to the contact increases. Thus, the increasing current elevates the occurrence of a low resistance contact, and this means that the major factor of forming a low resistance contact is electrical one. However, we note that when the current to the contact is very high, it is possible that the voltage measured in the contact is due to melting, not the tunneling.

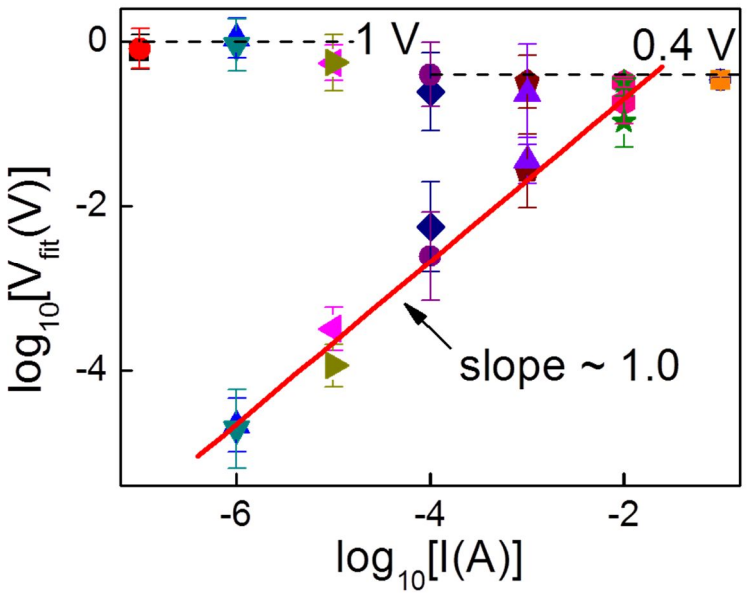

Figure 4.13 | The plot of mean voltage to current. Each symbol is the mean voltage coming from fitting line. The error bar is the standard deviation of fitting line.

For getting more statistical view of contact resistance with increasing current, we fit above each distribution to Gaussian distribution with two peaks. This is for obtaining the mean value and standard deviation of each distribution. Figure 4.13 is one plot to represent such statistical values. More easy view, we plot mean contact voltage with respect to current. The red line in the figure is the fitting line of low resistance mean values.

There are two points at each symbol, except for the cases of the current 0.1 μA and 100 mA. As shown in the figure 4.13, the contact state with low resistance shows Ohmic characteristic. This means that a low resistance contact formed by electrical field is a metal-metal bridge. And, the high resistance contact shows two aspects, which is why we plot the mean voltage with respect to the current. At low current, the mean voltage is about 1V, and at high current, it is saturated at the line of 0.4 V. We think that this is due to the difference of contact state. One is tunneling state, the other is melting state.

4.5 Dependence on an oxide layer thickness

To get more information about a tunneling state, we oxidize the stainless steel ball by thermal treatment. And we performed XPS depth profile for the information of thickness, ingredients about the oxide layer. Using these annealing balls, we implemented the experiment for obtaining the distribution of electrical contact resistance and dielectric breakdown voltage.

4.5.1 XPS data of Type 304 Stainless steel plate in different annealing

Figure 4.14 is the result of XPS depth profile of Type 304 stainless steel plate with respect to different thermal treatment that is same with that of both two stainless steel balls. The thermal treatment is (a) 200 ℃ during 1 hour, (b) 200 ℃ during 2 hours, (c) 300 ℃ during 1 hour, and (d) 300 ℃ during 2 hours, and it is heated in usual air. Though it is not easy to define the thickness as well as ingredients of the oxide layer, we define the thickness of oxide layer by the oxygen symbol where the slope changes greatly. In such definition, the oxide thickness in each case is about 2.5 nm, 2.5 nm, 3 nm, and 4 nm in alphabet order of figures. Even if the change in the case of 200 ℃ is little, the higher temperature and the longer time the thermal treatment applies, the thicker the oxide layer is.

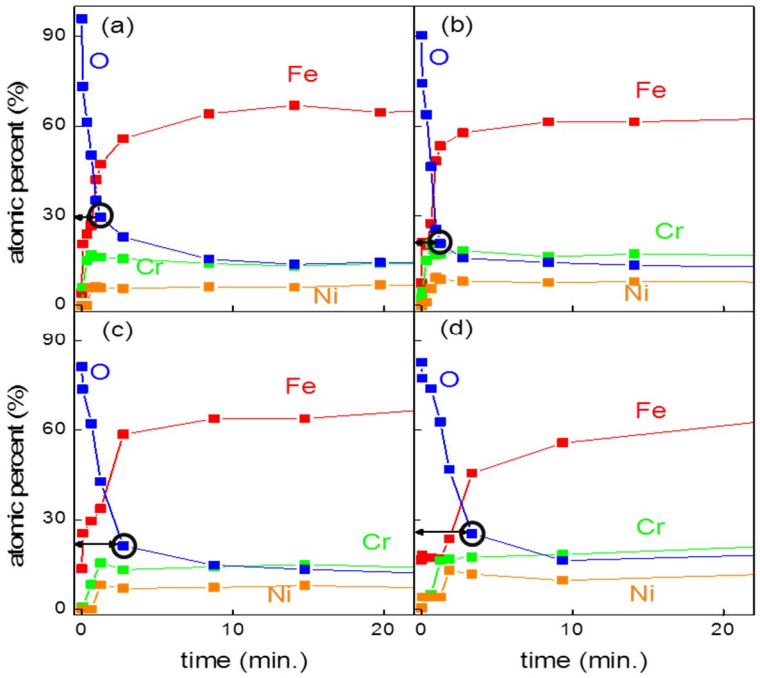

Figure 4.14 | XPS depth profile of stainless steel with respect to thermal treatment. As the temperature is higher and time of thermal treatment is longer, the thickness of oxide layer is thicker.

4.5.2 The variation of Dielectric breakdown voltage with respect to oxide layer thickness

In the beginning, we expected that a high resistance contact was due to the existence of the oxide layer on the surface of contact member. For identifying this expectation, we thickened the oxide layer on the surface, and how thick it is examined by XPS depth profile. Figure 4.15 is the distribution of electrical contact resistance with increasing an oxide layer thickness on the surface. This shows a distinct difference from the figure 4.2.

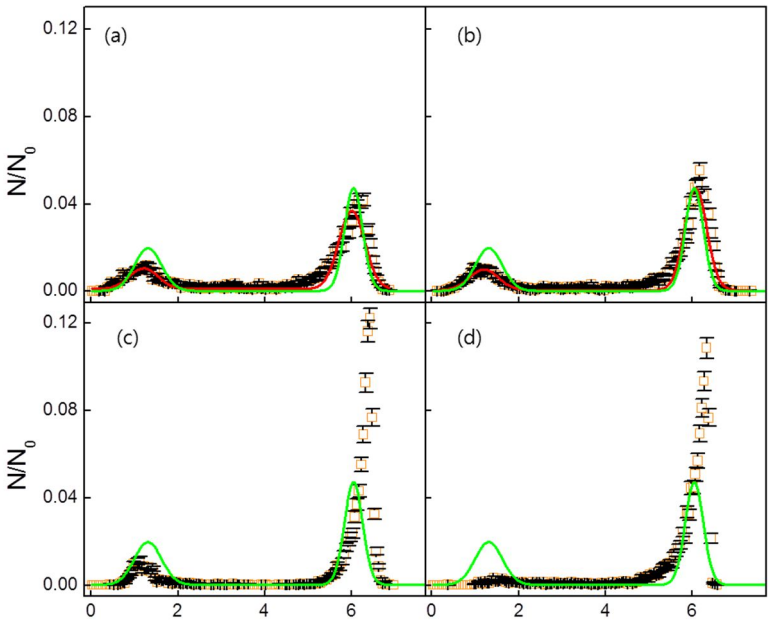

Figure 4.15 | The distribution of electrical contact resistance with respect to an oxide layer thickness. As the oxide layer is thicker, the appearance of a low resistance is reduced and that of the high resistance increased.

Figure 4.15 is also the histogram of contact resistance. The bar of the symbol is the expected statistical error, $\sqrt{n}$. The green line in the figure 4.15 is the Gaussian fitting line with two peaks of the distribution of resistance at current 1 μA, for comparing to other result. The red line is the Gaussian fitting line with two peaks of each distribution, except for (c), (d). In the figure 4.15 (c) and (d), we cannot fit the Gaussian line with two peaks to the distribution, because it is the rare occurrence of a low resistance contact state, which means that one peak in the distribution is disappeared, and the distribution in the high resistance portion is inappropriate to the Gaussian line, it is asymmetric shape, as seen by the right part cut in the distribution.

According to this result, the occurrence of a low resistance contact is dependent on the oxide layer on the surface. With increasing the thickness of the oxide layer, the frequency of a low resistance contact is rare, as shown in the figure 4.15. It is possible that the metal contact is not made by the contact load because of the thick oxide layer between contact sites. However, we identified that the metal contact is not formed even in the case of the stainless steel ball without thermal treatment. Thus, this result means that the thick oxide layer prevent the contact from dielectric breakdown. Considering that dielectric breakdown is dependent on the electric field, it is reasonable.

The asymmetry of distribution in the high resistance portion of figure 4.14 is also due to the enhanced robustness against dielectric breakdown. Dielectric breakdown may occur at the nearest site between contact surfaces. By thermal treatment, this nearest gap is far from each other than before. This means that these gaps become to be tunneling states. Furthermore, the voltage where dielectric breakdown occur is higher than before. In that case, the contact can hold more

voltage without dielectric breakdown. But, the high voltage can cause forming a partial bridge, by which two contact members are not connected perfectly, to the contact. That is soft dielectric breakdown. Thus, the high resistance contact is changed into the lower resistance state, which still has high resistance. This is why the high resistance portion in the figure 4.15(c), (d) shows an asymmetry distribution.

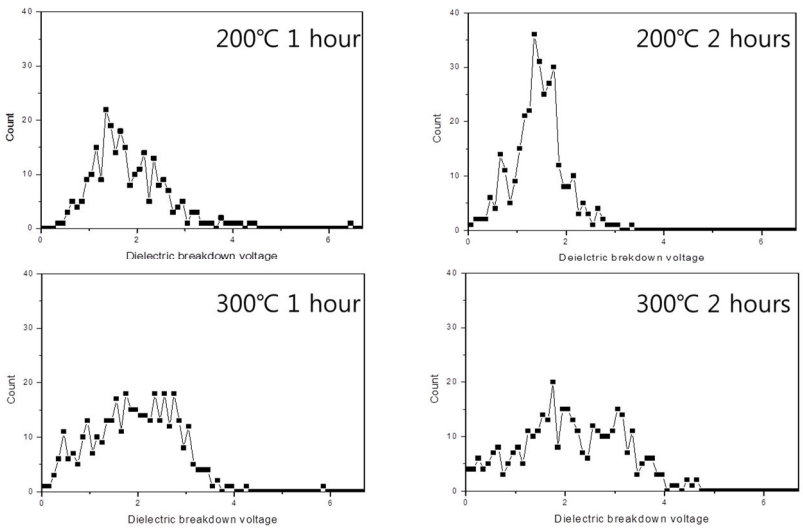

Figure 4.16 | the distribution of breakdown voltage with respect to an oxide layer thickness. The mean value of breakdown voltage is increased with oxide layer thickness.

Figure 4.16 is the distribution of a breakdown voltage from I-V measurements of each stainless steel ball with different thermal treatment. It is the same method with the method getting the data of figure 4.9. In the case of thermal treatment of 200℃ to the stainless steel ball, it is not much different from the case of a usual stainless steel ball except for the small shift of mean value toward high voltage. But, in the case of thermal treatment of 300℃ to the stainless steel ball, it is much different from the other cases. The voltage is distributed widely, comparing with the other cases. And the median or mean value is moved toward high voltage.

This result is consistent with the result of XPS depth profile and the distribution of electrical contact resistance. In the fig. 4.14(a) and (b), it is not much different from fig. 4.4. On the contrary, fig.4.14(c) and (d) is much different from fig. 4.4. This means that the surface state do not affected by the thermal treatment performed at 200℃, while the thermal treatment performed at 300℃ changed the surface state of the stainless steel, comparing with the no thermal treatment case. Also, the distribution of electrical contact resistance resulting from stainless steel ball annealed at 200℃ is similar to that resulting from usual stainless steel ball. On the contrary, the distribution of electrical contact resistance resulting from stainless steel ball annealed at 300℃ shows that low resistance contact is rarely appeared.

4.5.3 Post-breakdown Resistance and severity

It is reasonable that a post-breakdown resistance is related to the dielectric breakdown voltage. That is, the higher a dielectric breakdown voltage is, the lower the post-breakdown resistance is. And as the oxide layer is thicker, the voltage of dielectric breakdown voltage is higher.

Figure 4.17 shows that the experimental result accord with such expectation when the dielectric breakdown occurs at high voltage. And in common with fig. 4.10, the post-breakdown resistance is widespread from 10 Ω to tens-of-k Ω when the dielectric breakdown occurs at a low voltage. However, in the case of 300℃, the post − breakdown resistance tends to spread through the whole voltage level. We think that this is due to the thicker oxide layer. The thicker oxide layer elevates the voltage of dielectric breakdown. Thus, the spread of post − breakdown resistance is appeared in the higher voltage.

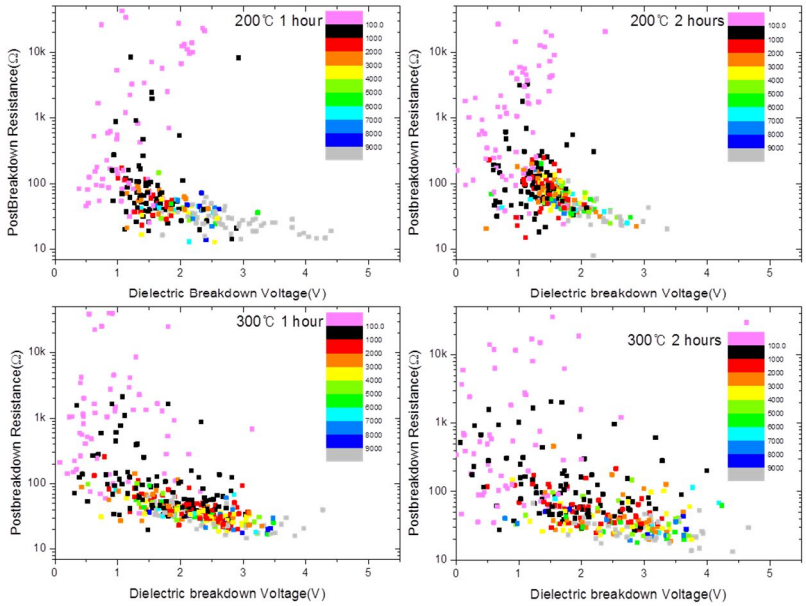

Figure 4.17 | The relation between dielectric breakdown voltage and Post-breakdown resistance. As the oxide layer is thicker, the low severity of breakdown spread out toward high dielectric breakdown voltage.

4.6 Dependence on the atmosphere

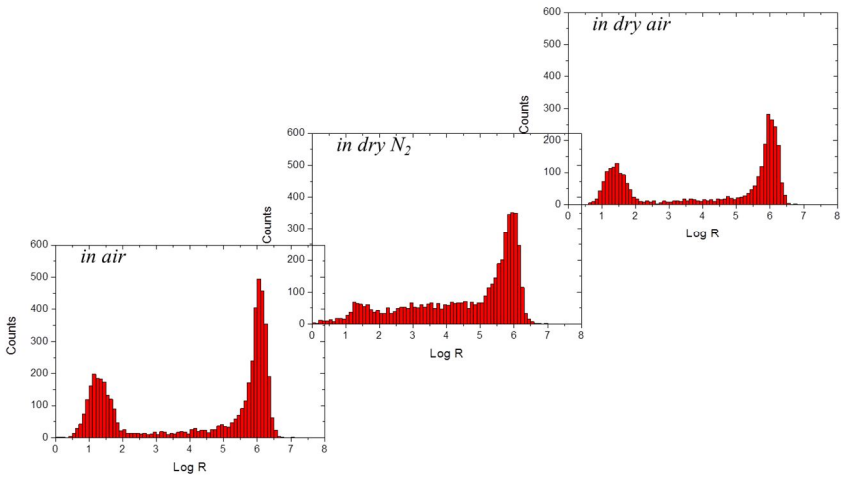

Figure 4.18 | The variation of distribution by changing atmosphere. According to the existence of oxygen in air, the distribution of electrical contact resistance is varied. This is due to the recovering of oxide layer on the surface

The distribution of electrical contact resistance is varied by the atmosphere. The main ingredient causing the variation is the oxygen. The other ingredients in atmosphere do not affect the distribution, severely.

Figure 4.22 shows the variation of resistance with respect to the atmosphere composition. At First, the electrical contact resistance measured in air. Then, the electrical contact resistance of the same balls was measured in the container which was filled with dry N_2 and kept dry N_2 flowing. At last, identifying whether the stainless steel ball was permanently damaged by the dry N2 gas, the electrical contact resistance of these balls was measured in same condition of first

measurement. The result in the fig. 4.22 implies two infers about the relation of electrical contact resistance to air composition. One is that the existence of oxygen in atmosphere affects the distribution of electrical contact resistance, severely. Another is that the contact does not get a permanent damage by air. According to these two infers, we suggest that when the oxide layer on the surface of the contact members is partially destroyed by electric field, it is quickly recovered by oxygen in air.

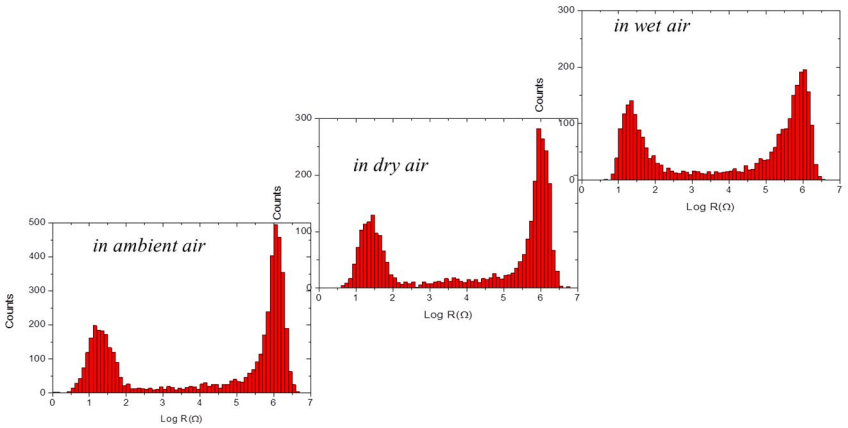

Figure 4.19 | The variation of the distribution according to humidity in air. There is a small variation by changing the humidity.

The other ingredient in air, such as the water vapor, does not affect the distribution of electrical contact resistance, drastically. Figure 4.23 shows that the

distribution is much changed by the concentration of water vapor in. Thus, the existence of oxygen in air is a meaningful factor affecting the distribution of electrical contact resistance than the other composition in air.

4.7 The result of simulation

The simulation is implemented for identifying the distribution of the conducting path formed by a dielectric breakdown. It is designed on the foundation of a random resistor network model. The resistor within the network model is two types, which have low and high resistance. They represent the defect inside the layer and the insulating material, and the resistor with high resistance can be changed into one with low resistance at a certain condition. The condition is that the electric field applying to the resistor is larger than a threshold value.

4.7.1 Distribution

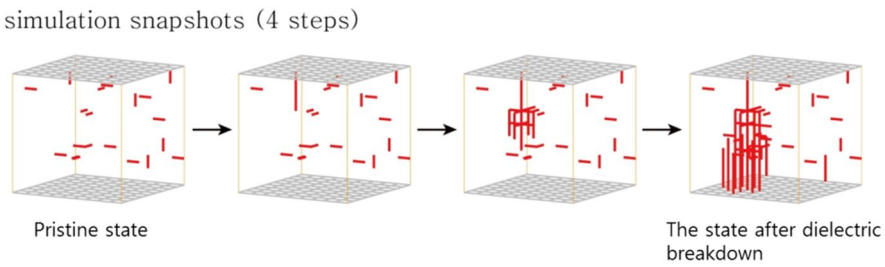

Figure 4.20 | 4 snapshots of simulation. This show the growth of the filament which connects between two sides.

Figure 4.18 is Simulation snapshots of 4 steps, which are composed of a pristine state, two middle states, and a final state. A thin oxide layer is represented by the resistor network, which is composed of all a high resistance one. But, there exist some defects, like impurities or lattice deficiency, in the real oxide layer, and they play a role of conducting material. In our case, they are represented by a low resistance resistor in the resistor network. A red bond is a low resistance resistor. We give some fraction of defects in pristine state.

When a high voltage larger than a threshold value is applied to a high resistance resistor, the resistor is changed into a low resistance resistor. In the middle of simulation, the red bond increases in the resistor network, gradually. And we can observe the growing a low-resistor's filament in the network. Finally, the filament crossed between top and bottom electrode occurs. The initial high resistance contact is changed into the final low resistance contact.

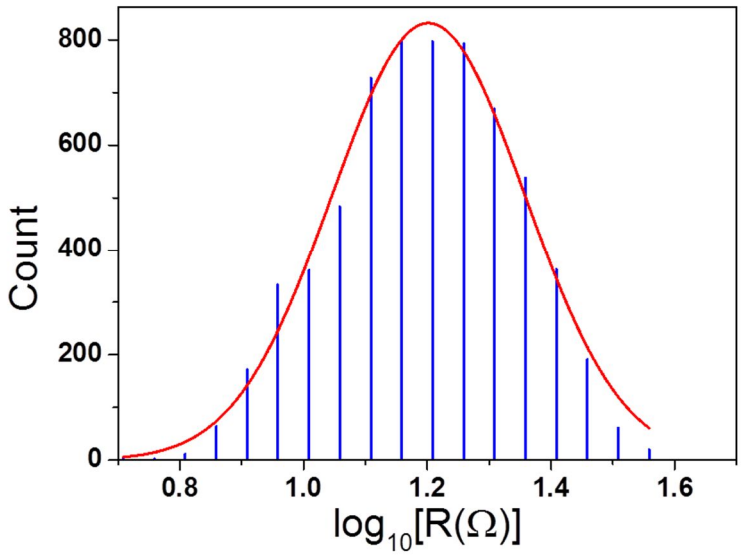

Figure 4.21 | the distribution of the resistance of conduction path formed by simulation. This resistance distribution in simulation is similar to that in the experimental data.

However, the low resistance network is not always formed. Among total 20000 simulations, the number of the formed low resistance network is 6388. This result is agreement to our experimental result, except for the current. But it is not a meaningful problem, just the problem of condition control like a resistor value. Figure 4.19 is the distribution of the network's total resistance in the case of forming conduction path. It shows a log-normal distribution same with our experimental result.

The result that the distribution of the network's total resistance with conduction path is a log-normal distribution is not changed in another initial defect ratio. The variation with respect to the initial defect ratio is the distortion degrees of the tail in the log-normal distribution. It is a very interesting point that the distribution of the resistance of conduction paths formed by a dielectric breakdown is a log normal distribution.

4.7.2 I-V characteristic

Figure 4.21 is two I-V results of simulation at above network model. This is also agreement to our experimental result. The direction of I-V is ascending along with (1), and descending along with (2). The red symbol shows a severe dielectric breakdown which means that the one thick bridge or many paths is formed between top and bottom electrode. In that case, the total resistance of the network is very low and the charge is not retained in other site of contact surface because of this good conduction passage. This implies us the perfect dielectric breakdown which means that a dielectric breakdown does not occur in that state any more.

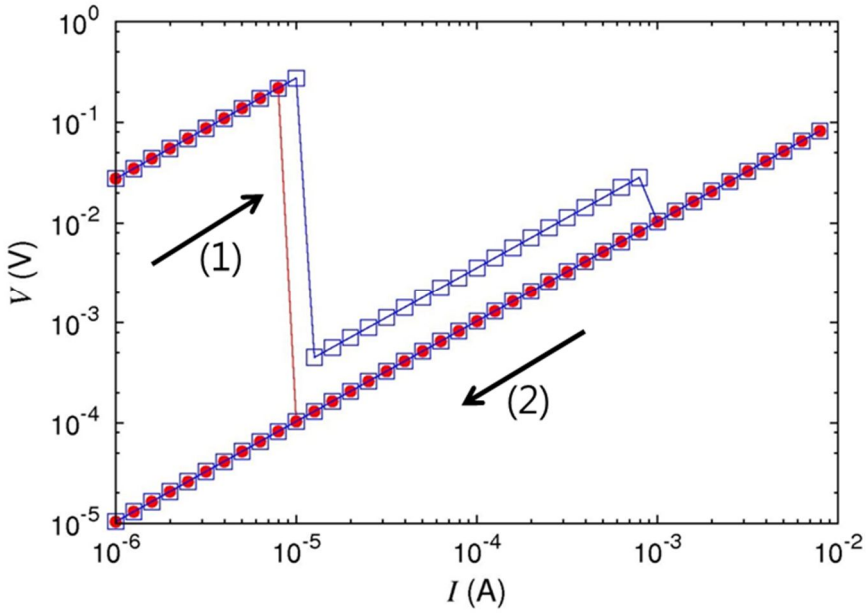

Figure 4.22 | I-V measurements by simulation. This I-V characteristic is similar to that in the experiment.

On the contrary, a blue symbol shows the existence of an imperfect dielectric breakdown. There are two points, where its voltage drops, in the graph of the blue symbol. The first point is more severe than the second one. However, it is less severe than that of the red symbol. And the drop degree of the second point is small, relatively. This means that even if a dielectric breakdown occurs, the other site of the contact surface can charge and grow another filament by high electric field applied to that site.

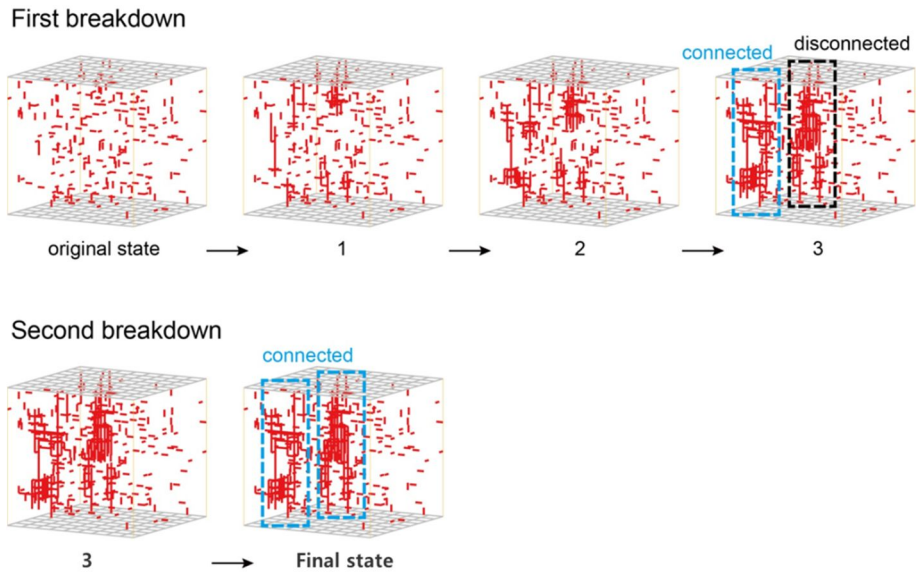

Figure 4.23 | the snapshots of blue symbol in the figure 4.18. This shows that it is possible for multiple conducting filaments to be formed in the MIM structures.

Our former supposition can identify by snapshots of I-V simulation. Figure 4.22 is the snapshots of the blue symbol in the figure 4.21. There are some defects in the original state, for reality. As the current increases, the red bond increases at random site. However, if some clusters begin to be appeared in the network, those clusters are growing with increasing current, independently. Then, some clusters, inside which clusters extending from two electrode exist, are connected each other, and the conducting paths crossing between two electrode is formed. This delineation about growing filament can be seen in the images numbered by 1, 2, 3 of figure 4.22.

If conducting paths formed by a dielectric breakdown is thin as shown in the blue box of figure 4.22, the defects arises from the high electric field, which is due to imperfect current flow between two electrodes. As shown in the image numbered by 3 of figure 4.22, another two clusters exist growing which is respectively extended from top and bottom electrode, but they are not connected each other. In the final state, they are connected. It means that another dielectric breakdown differing from former occurs.

Chapter 5

Conclusion

In summary, we studied the distribution of electrical contact resistances of two stainless steel balls arranged in a vertical array and found that the data points clustered primarily into two groups. One group corresponds to tunneling conduction, and the other group is due to the conduction through bridges formed from the breakdown of the oxide layer of the contact. The tunneling contacts show a log-normal peak and a wide spread of resistances due to the fluctuation of the distance of the site where the contacting surfaces are closest to each other by mechanical or electrical parameter and the tunneling occur. The bridged contacts by dielectric breakdown also show log-normal distributions due to the formation of conducting filaments. We conclude that the electrical contacts possess complex behavior due to their inherent microscopic inhomogeneity and the unpredictable deformations during the course of the measurements. A statistical analysis with a sufficient number of measurements and a new simulation model supporting such results is essential for the study of contacts.

There is another condition to affect the electrical contact resistance. The slow change of electrical contact resistance with time evolution was observed. By experiment, this is not due to external parameters, such as the current from external source and the load pressing the contact. We suggest that the slow variation of the

inside factor such as the position of the grain boundary inside the oxide layer causes the slow change of the electrical contact resistance. Furthermore, we observed that the electrical contact resistance depends on the atmosphere. Specially, the existence of oxygen in air is an important factor causing the variation of the distribution than the other ingredients in air. We suggest that it is due to the effect of quickly recovering an oxide layer on the surface when it is damaged by electric field.

Bibliography

[1] C.M. Doelling, T.K. Vanderlicka, J. Song, and D. Srolovitz, J. Appl. Phys., **101**, 124303 (2007).

[2] H. Seehase, IEEE Trans. Rel. , **40**, (2007).

[3] L. Kogut, Electrical performance of contaminated rough surfaces in contact, J. Appl. Phys., **97**, 103723 (2005).

[4] C.N. Neufeld, and W.F. Rieder, Electrical Characteristic of Various Contact Contamination IEEE Trans. Comp. Pack. Technol., **18**, 369 (1995).

[5] R. Schubert, Degradation and regeneration of copper eletrical junctions, Phys. Rev. B, **43**, 1433 (1991).

[6] 안세나, Time evolution of granular particles confined in 2-dimensional box, Seoul Nation University Master's Thesis, (2004).

[7] 이종진, Study on the motions in confined granular systems, Seoul National University doctor's Thesis, (2004).

[8] 최춘희, 막 쌓인 쇠공의 전기 저항이 시간에 따라 변화하는 특성, Seoul National University Master's Thesis, (1998).

[9] R. Behringer, and J. Jenkins, *Powders & Grains '97* (Balkema, Rotterdam, 1997).

[10] J.G. Greenwood, Brit. J. Appl. Phys., **Vol.17**, 1621 (1966).

[11] J.G. Greenwood, and J.B.P. Williamson, Proc. R. Soc. London, Ser. A 295, **295**, 300 (1966).

[12] R. Holm, *Electrical Contacts* 4th ed.(Springer-Verlag, Belrin, 1967).

[13] B. Nikolć, and P.B. Allen, Electron transport through a circular constriction, Phys. Rev. B, **60**, 3963 (1999).

[14] Y.V. Sharviin, JETP **48**, 984 (1965).

[15] R.S. Timsit, IEEE Trans. Comp. Pack. Technol., Vol . 22, 85 **Vol. 22**, 85 (1999).

[16] R.S. Timsit, Electrical conduction through small contact spots, IEEE Trans. Comp. Pack. Technol., **29**, 727 (2006).

[17] J.W. Tringe, T.A. Uhlman, A.C. Oliver, and J.E. Houston, A single asperity and of Au/Au electrical contacts, J. Appl. Phys., **93**, 4661 (2003).

[18] G. Wexler, Proc. Phys. Soc., **89**, 927 (1966).

[19] D. Erts, H. Olin, L. Ryen, E. Olsson, and A. Thölén, Maxwell and Sharvin conductance in gold point contacts investigated using TEM-STM, Phys. Rev. B, **61**, 12725 (2000).

[20] M. Brandbyge, J. Schiøtz, M.R. Sørensen, P. Stoltze, K.W. Jacobsen, and J.K. Nørskov, Quantized conductance in atom-sized wires between two metals, Phys. Rev. B, **52**, 8499 (1995).

[21] K.S. Chan, and J.H. Wei, Quantum Ballistic transport in nanowire junctions, Phys. Rev. B, **75**, 125310 (2007).

[22] Y.-F. Lin, and W.-B. Jian, Nano Lett., **8**, 3146 (2008).

[23] G. Rubio, N. Agraït, and S. Viera, Atomic-sized metallic contacts: Mechanical properies and Electronic Transport, phys. Rev. Lett., **76**, 2302 (1996).

[24] E. Scheer, P. Joyez, D. Esteve, C. Urina, and M.H. Devoret, Conduction channel transmission of Atomic-size Aluminum contacts, phys. Rev. Lett., **78**, 3535

(1997).

[25] K.M. Schep, P.J. Kelly, and G.E.W. Bauer, Ballistic transport and electronic structure, Phys. Rev. B, **57**, 8907 (1998).

[26] T. Schwamb, B.R. Burg, N.C. Schrimer, and D. Poulikakos, On the effect of the electrical contact resistance in nanodevices, Appl. Phys. Lett., **92**, 243106 (2008).

[27] J.A. Torres, and J.J. Sáenz, Conductance mechanical properties of Atomic size metallic contacts: a simple model, phys. Rev. Lett., **77**, 2245 (1996).

[28] L. Olessn, E. laegsgaard, I. Stensgaard, F. Besenbacher, J. Schiøtz, P. Stoltze, K.W. Jacobsen, and J.K. Nørskov, Quantized conductance in an Atom-sized point contact, **72**, 2251 (1994).

[29] J.I. Pascual, J. Méndez, J. Gómez-Herrero, A.M. Baró, and N. Garía, Quantum contact in gold nanostructure by scanning tunneling Microscopy, phys. Rev. Lett., **71**, 1852 (1993).

[30] K.L. Johnson, *Contact Mechanics* (Cambridge University Press, Cambridge, 1985).

[31] B.N.J. Persson, Elastoplastic contact between randomly rough sufaces, Phys. Rev. Lett., **87**, 116101 (2001).

[32] W. Yan, and K. Komvopoulos, J. Appl. Phys., **84**, 3617 (1998).

[33] C. Yang, and B.N.J. Persson, Molecular dynamics study of contact mechanics: contact area and interfacial separation from small to full contact, phys. Rev. Lett., **100**, 024303 (2008).

[34] B.N.J. Persson, Relation between interfacial separatioin and load: A general theory of contact mechanics, phys. Rev. Lett., **99**, 125502 (2007).

[35] L. Kogut, and K. Komvopoulos, J. Appl. Phys., **94**, 3153 (2003).

[36] J.G. Simmons, , J. Appl. Phys., **34**, 2481 (1963).

[37] L. Kogut, and K. Komvopoulos, J. Appl. Phys., **95**, 576 (2004).

[38] T.W. Hickmott, Formation of Ohmic contacts: A breakdown mechanism in metal-insulator-metal structures, J. Appl. Phys., **100**, 083712 (2006).

[39] D.M. Schaefer, P.F.P. Fichtner, M. Carara, L.F. Schelp, and L.S. Dorneles, Dielectric breakdown in AlO_x tunneling barriers, J. Phys. D: Appl. Phys. , **44**, 135403 (2011).

[40] L. Kogut, and K. Komvopoulos, Breakdown of ultrathin native oxide films at contact interfaces of electromechancially stressed silicon microdevices, J. Appl. Phys., **97**, 124102 (2005).

[41] L. Niemeryer, L. Pietronero, and H.J. Wiesmann, Phys. Rev. Lett., **52**, 1033 (1984).

[42] M. Murat, Phys. Rev. B, **32**, 8420 (1985).

[43] J.S. Lee, S.B. Lee, S.H. Chang, L.G. Gao, B.S. Kang, M.-J. Lee, C.J. Kim, T.W. Noh, and B. Kahng, Scaling theory for unipolar resitance switching, Phys. Rev. Lett., **105**, 205701 (2010).

[44] G.I. Meijer, Who wins the Science, **319**, 1625 (2008).

[45] M.-J. Lee, S. Han, S.H. Jeon, B.H. Park, B.S. Kang, S.-E. Ahn, K.H. Kim, C.B. Lee, C.J. Kim, I.-K. Yoo, D.H. Seo, X.-S. Li, J.-B. Park, J.-H. Lee, and Y. Park, Electrical Manipulation of Nanofilaments in Transition-Metal Oxides for Resistance-Based Memory, Nano Lett., **9**, 1476 (2009).

[46] D.-H. Kwon, K.M. Kim, J.H. Jang, J.M. Jeon, M.H. Lee, G.H. Kim, X.-S. Li, G.-S. Park, B. Lee, S. Han, M. Kim, and C.S. Hwang, Atomic structure of

conducting nanofilaments in TiO2 resistive switching memory, Nature Nanotechnology, **5**, 148 (2010).

[47] M.J. Rozenberg, I.H. Inoue, and M.J. Sánchez, Nonvolatile Memory with, Phys. Rev. Lett., **92**, 178302 (2004).

[48] R. Waser, and M. Aono, Nanoionics-based resistive, Nater Mater., **6**, 833 (2007).

[49] J. Yao, Z. Sun, D. Natelson, and J.M. Tour, Resistive switches and, Nano Lett., **10**, 4105 (2010).

[50] J.J. Yang, M.D. Pickett, X. Li, D.A.A. Ohlberg, D.R. Stewart, and R.S. Williams, Memristive switching mechanism, Nater Nanotechnology, **3**, (2008).

[51] G. Betz, G.K. Wehner, L. Toth, and A. Joshi, J. Appl. Phys., **45**, 5312 (1974).

[52] W. Yang, G. Zhao, M. Zhang, and J. Congleton, An AES investicgation of the surface films Formed on stress corrosion test specimens of type 304 stainless steel in high temperature water, Corrosion Science, **33**, 89 (1992).

[53] C.-O.A. Olsson, and D. Landolt, Passive films on stainless steels-chemistry, structure and growth, Electrochimica Acta, **48**, 1093 (2003).

[54] J.B. Barber, Bounds on the electrical resistance between contacting elastic rough bodies, Proc. R. Soc. Lond. A, **459**, 53 (2003).

[55] M. Ciavarella, S. Dibello, and G. Demelio, Conductance of rough random profiles, Solid and Structures, **45**, 879 (2008).

[56] A. Mikrajuddina, F.G. Shib, H.K. Kimb, and K. Okuyamaa, Size-dependent electrical constriction resistance for contacts of arbitrary size: from Sharvin to Holm limits, Materials Science in Semiconductor Processing, **2**, 321 (1999).

[57] Y.G. Naidyuk, and I.K. Yanson, *Point-contact spectroscopy* (spriger, New York,

USA, 2005).

[58] M.R. D., IEEE Trans. Compon. Hybrid. Manuf. Technol., **15**, 339 (1992).

[59] N. M., IEEE Trans. Compon. Hybrid. Manuf. Technol., **18**, 382 (1994).

[60] B. L., IEEE Trans. Compon. Hybrid. Manuf. Technol., **24**, 50 (2001).

[61] M. Ciavarella, V. Delfine, and V. Demelio, A new 2D asperity model with interaction for studying the contact of multiscale rough random profiles, wear, **261**, 556 (2006).

[62] M. Ciavarella, G. Murolo, and G. Demelio, The electrical/thermal conductance of rough surfaces-The Weierstrass-Achard multiscale model, International Journal of Solids and Structures, **41**, 4107 (2004).

[63] R.L. Jackson, and J.L. Streator, A multi-scale model for contact between rough surfaces, wear, **261**, 1337 (2006).

[64] Y.H. Jang, and J.R. Barber, Effect of contact statistics on electrical contact resistance, J. Appl. Phys., **94**, 7215 (2003).

[65] S. Lee, H. Cho, and Y.H. Jang, Mulltiscale electrical contact resistance in clustered contact distribution, J. Appl. Phys., **42**, 165302 (2009).

[66] D.J. Griffiths, *Introduction to Quantum mechanics, 2nd ed.(Person Education, Inc., New jersey, 2005)* (Person Education, Inc., New jersey, 2005).

[67] F. Bardou, Europhys. Lett., **39**, 239 (1997).

[68] V.K. Costa, F. Bardou, C. B´eal, Y. Henry, J.P. Bucher, and K. Ounadjela, J. Appl. Phys., **83**, 6703 (1998).

[69] E.L. Crow, and K. Shimizu, *Lognormal distributions : Theory and applications* (Marcel Dekker, INC, New York, 1988).

[70] R.S. Timsit, The melting voltage in elecric contacts, IEEE Trans. Comp. Hybrid. Manuf. Technol., **14**, 285 (1991).

[71] M. Housaa, T. nigam, P.W. Mertens, and M.M. Heyns, Model for the current J. Appl. Phys., **84**, 4351 (1998).

[72] D.F. Farson, H.W. Choi, and S.I. Rokhlin, electrical discharges between, Nanotechnology, **17**, 132 (2006).

[73] J. Suñé, I. Placencia, N. Barniol, f. Martín, and X. Aymerich, on the breakdown statistics of very thin SiO_2 films, Thin Solid Films, **185**, 347 (1990).

[74] Y. Yagil, G. Deutscher, and D.J. Bergman, electrical breakdown measuremnts, phys. Rev. Lett. , **69**, 1423 (1992).

[75] A. Avellán, S. Jakchilk, B. Tippelt, S. Kudelka, and W. Krautschneider, post hard breakdown, IEEE Electron Dvice Letters, **29**, 366 (2008).

[76] R. Degraeve, B. Kaczer, and G. Groeseneken, Ultra-thin oxide, Microelectron Reliab., **40**, 697 (2000).

[77] E. Muiranda, and J. Suñé, electron transport through, Microelectron Reliab., **44**, 1 (2004).

[78] C.-H. Chen, J.A. Yeh, and P.-J. Wang, electrical breakdown phenomena, J. Micromech. Microeng., **16**, 1366 (2006).

[79] M.A. Alam, and B.E. Weir, A study of soft and Hard breakdown-, IEEE Trnas. Electron Devices, **49**, 232 (2002).

[80] J.S. Lee, Reversible percolation model: Its application to resistance switching phenomena, Seoul National University Doctor's Thesis, (2010).

[81] D. Stauffer, and A. Aharony, *Introducton to Percolation theory* (Taylor & Francis Inc, Philadelphia, 2003).

[82] S. Kirkpatrick, Percolation and conduction, Review of Modern Physics, **45**, 574 (1973).

[83] J. Boksiner, and P.L. Leath, Dielectric breakdown in media with defects, phys. Rev. E, **57**, 3531 (2998).

[84] S.S. Manna, and B.K. Chakrabarti, Dielectric breakdown in the presence of random conductors, Phys. Rev. B, **36**, 4078 (2987).

[85] J.P. Straley, and S.W. Kenkel, Percolation theory for nonlinear conductors, Phys. Rev. B, **29**, 6299 (2984).

[86] P.A. Lee, Variable range hopping in finite, Phys. Rev. Lett., **53**, 2042 (1984).

[87] M.M. Fogler, and R.S. Kelley, Non-Ohmic Variable, Phys. Rev. Lett., **95**, 166604 (2005).

[88] V. Ambegaokar, B.I. Halperin, and J.S. Langer, Hopping conductivity in disordered system, Phys. Rev. B, **4**, 4 (1971).

[89] H. Kwak, Study on Statistcal properties of contact resistance in two stainless(SUS 304) bearing contact, Seoul National University Master's Thesis, (2009).

국문 초록

접촉 전기 저항은 접촉을 이루는 물체의 전기 저항 비와 접촉 면적, 접촉모양과 같은 접촉에 발생하는 변수에 의존한다. 그렇지만, 접촉 힘이 접촉 사이에 얇은 산화 막이 존재할 수 있을 정도로 매우 작다면 접촉 전기 저항은 복잡한 양상을 띄게 된다.

약한 접촉에는 두 가지 전기적 상황이 존재한다. 하나는 높은 저항을 가지는 접촉이고 다른 하나는 낮은 저항을 가지는 접촉이다. 약한 접촉에서 발생하는 높은 저항은 접촉 사이에 존재하는 산화 막 때문이다. 고전 전자기역학에서는 산화 막을 통한 전자 흐름을 설명하기는 어렵다. 그렇지만 양자 역학에서는 산화 막 넘어 전자를 발견할 확률이 어느 정도 있다고 말하고 그러한 현상을 tunneling 효과라 한다. 투널 (Tunneling) 전기 저항은 금속의 전기 저항에 비해 매우 높다. 그렇기 때문에 높은 저항 접촉은 투널 효과의 산물이라고 볼 수 있다. 낮은 저항 접촉은 접촉 사이에 산화 막을 가로 지르는 전기 흐름 길이 생성으로 발생한 것이다. 만약 접촉에 가하는 힘이 산화 막을 파괴할 수 있을 정도로 크다면 접촉 전기 저항은 실제 만들어지는 전기 접촉의 특성으로 결정될 것이다. 그렇지만 약한 접촉의 경우에서는 접촉 사이에 얇은 산화 막이 존재한다. 그런 경우에 접촉 사이에 존재하는 산화 막은 전기적 충격으로 파괴될 수 있다. 그러한 현상은 유전체 파괴(dielectric breakdown) 이라고 한다.

얇은 산화 막으로 분리된 접촉은 전기 전도 현상을 연구하기 위해 스테인리스 스틸 볼 접촉의 전기 저항을 측정하였다. 접촉 전기 저항을

5000번까지 반복적으로 측정하였을 때, 그것은 분포는 두 개의 평균 값을 가지는 로그 노말 분포(bimodal log−normal distribution)을 이룬다. 높은 저항 평균 값은 1 MΩ 으로 그것은, 앞서 말했듯이, 산화 막을 통한 투널 전도 때문이다. 반면에, 낮은 저항 접촉은 산화 막을 가로지르는 전기 흐름 길이 생성되었기 때문에 발생하고 그러한 접촉의 평균 저항은 10 Ω 정도 된다. 그러한 전기 흐름 길 생성은 접촉 사이 전압이 1 V 이상이 되었을 때 발생한다. 이 결과는 낮은 저항 접촉은 접촉 사이 역학적 변수와 상관없이 전기적 변수만으로도 발생할 수 있음을 보여 준다.

랜덤 저항 네트워크 (random resistor network) 모델에 회로 차단기(circuit breaker)를 추가해서, 낮은 저항 상황을 구현하였다. 이러한 시뮬레이션에서 낮은 저항 접촉의 전기 저항은 전기적으로 유도된 필라멘트 집합체의 전기 저항으로 바꿔 볼 수 있다. 그것은 기존의 접촉 전기 저항을 추정할 때 쓰이던 Holm 이나 Sharvin의 식과는 다른 것이다. 우리는 그렇게 추정한 접촉 전기 저항 결과들이 적절한 시뮬레이션 변수들을 설정하면 실제 실험과 일치함을 확인하였다. 특히, 접촉 전기 저항의 분포가 시뮬레이션 변수 설정과 상관없이 시뮬레이션에서도 보인다는 점은 우리의 해석이, 즉, 낮은 저항 접촉이 역학적인 아닌 전기적으로 생성될 수 있다는 가정이 틀리지 않았음을 보여 준다.

또한, 우리는 접촉 전기 저항에 영향을 주는 다른 변수들을 찾기 위한 추가적인 실험을 했다. 그러한 실험들은 통해, 접촉 전기 저항이 시간에 따라 천천히 변한다는 사실을 알았다. 이것은 접촉 힘이나 전기 흐름의 정도와 상관 없이 나타나는 현상으로, 전기 저항에 영향을 주는 산화 막 내부 변수의 시간에 따른 변화 때문에 발생하는 것으로 보고 있다. 예를

들어, 산화 막 내부에 존재하는 그레인 바운더리(grain boundary)에서는 그레인보다 전기 전도 성이 더 좋다. 산화 막 내분에서 이것의 위치가 시간에 따라 변한다면 접촉 전기 저항 역시 시간에 따라 변할 수 있다. 접촉 전기 저항에 영향을 주는 또 다른 변수로는 대기의 구성이다. 실험을 통하여 우리는 산소의 존재 여부가 낮은 저항 접촉의 생성과 관련이 있다는 사실을 알아 냈다. 이는 접촉 사이에 존재하는 산화 막의 복구가 공기 중에 존재하는 산소의 존재와 관련 있기 때문으로 추정하고 있다.

주요어: 접촉 전기 저항, 유전체 파괴, 무작위 저항 네트워크, 투널링 효과, 전도 성 필라멘트, 로그-노말 분포

학번: 2007-30778